Chapter 2 Literature Review

2.1 Metal–organic frameworks

MOFs are porous crystalline materials with hybrid frameworks built from the linkages of metal ions with organic linkers.[1-3] The functional groups of the organic linkers for coordinative bonding to the metal ions and the coordination geometry of the metal nodes (metal ions or metal-containing clusters) play a decisive role in the formation of the topologies of MOF structures. The appropriate groups are carboxylate, heterocyclic nitrogen, amine, nitrile, phosphonate and sulfonate (Figure 2.1).[4-8] Among them, carboxylate group is the most commonly used functionality for designing and constructing MOF structures.[9,10] Multitopic linkers (*i.e.,* containing two or more functional groups) with rigid carbon backbones favor prominently in the quest for stable and robust frameworks that retain MOF integrity in the absence of guest molecules. The rigid carbon backbones are usually aromatic chains or alkenyl chains with double bonds. Metalloligands are also used as linkers for the construction of MOFs.[11-16] Furthermore, the linkers can be flexible organic molecules, but in some cases they tend to give MOF structures in the form of dense packing or interpenetration.[17-19]

Ditopic linkers

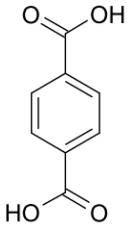

1,4-benzenedicarboxylic acid

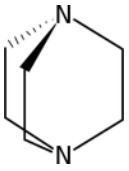

1,4-diaza-bicyclo[2.2.2]octane

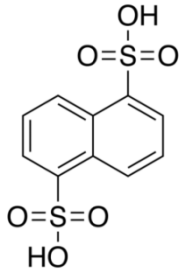

1,5-naphthalenedisulfonic acid

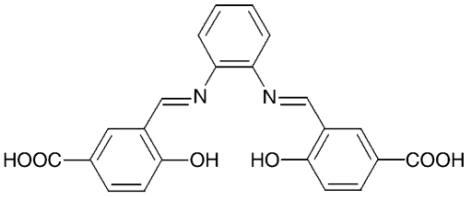

N,N′-phenylenebis(salicylideneimine)dicarboxylic acid

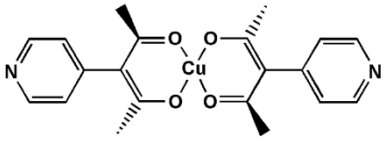

Bis[3-(4-pyridyl)pentane-2,4-dionato]copper(II)

Tritopic linkers

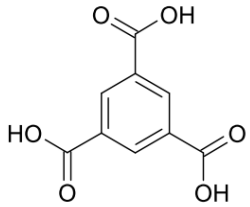

1,3,5-benzenetricarboxylic acid

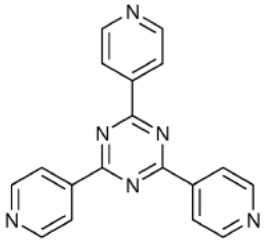

2,4,6-tris(4-pyridyl)-1,3,5-triazine

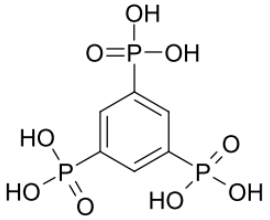

1,3,5-benzenetriphosphonic acid

Tetratopic linkers

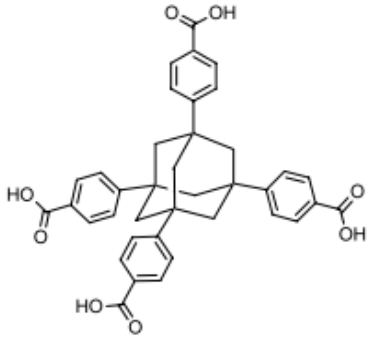

1,3,5,7-adamantanetetrabenzoic acid

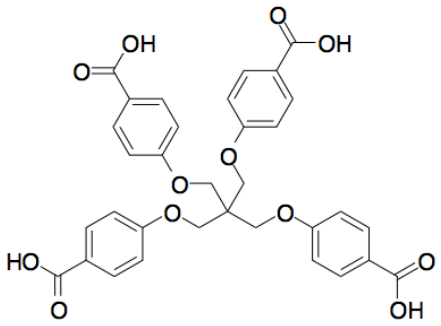

Tetrakis[4-(carboxyphenyl)oxamethyl]methane

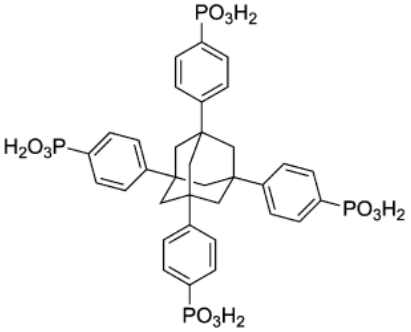

1,3,5,7-tetrakis(4-phosphonophenyl)adamantine

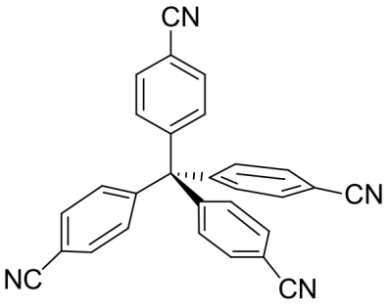

Tetrakis(4-cyanophenyl)methane

Figure 2.1 Multitopic organic linkers for MOF construction.[4-16]

The metal ions constructing MOF structures possess several coordination numbers. The first row transition metal ions such as Cr^{3+}, Fe^{3+}, Cu^{2+} and Zn^{2+} are widely used for constructing MOFs.[10,20] The coordination of the functional groups of organic linkers to the metal ions often generates polyatomic clusters containing two or more metal atoms, so-

called secondary building units (SBUs). The SBUs give points of extension where they connect to the rigid carbon backbones of the organic linkers to form porous structures. The geometry of the SBUs is determined by the coordination number, coordination geometry of the metal ions and the nature of the functional groups. The variety of SBU geometries with different numbers of points of extension has been observed in MOF structures.[10,21] However, the metal-containing SBUs are not isolatable entities, and so it is essential to establish exact chemical conditions that will yield a specific SBU *in situ*.[8]

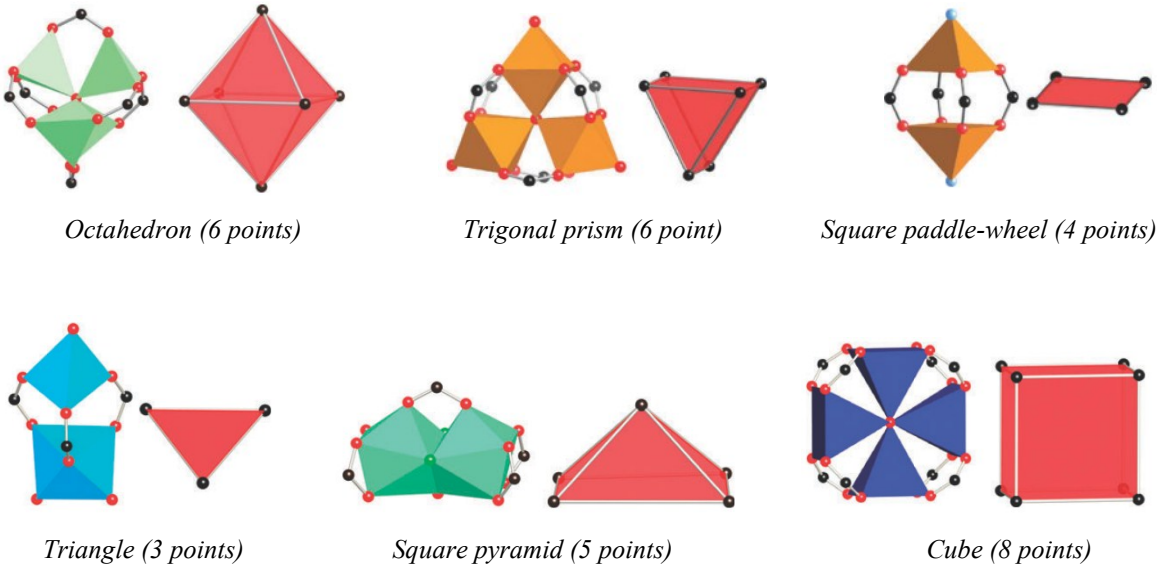

Figure 2.2 Geometry and number of points of extension of representative SBUs. Metal: polyhedral; C: black; O: red; Heteroatom: green, cyan. Reproduced with the permission of The Royal Society of Chemistry.[10]

The most common SBUs are clusters of metal ions and carboxylate groups. The typical examples are octahedral, trigonal prism and square paddle-wheel SBUs (Figure 2.2).[10] The octahedral SBU with the formula of $M_4O(COO)_6$ consists of a central bridging O atom bonding to four tetrahedral metal atoms to form a tetrahedral M_4O unit; and six carboxylate groups connecting the edges of the tetrahedra. The six points of extension (*i.e.,* six carbon atoms of the carboxylate groups) are at the vertices of the octahedron. This cluster is found for Zn, Co and Be. In case of trigonal prism SBU with the formula of $M_3O(COO)_6$, three metal ions connect together via a central bridging O atom and each pair of the octahedral

metal atoms is bridged by two carboxylate groups. Each metal ion coordinates to a terminal ligand such as solvent or anion. The six points of extension locate at the vertices of the trigonal prism. This SBU is observed for several metals such as Cr, Fe and Al. In the square paddle-wheel SBU, two metal ions are bridged by four carboxylate groups and each metal ion is coordinated by a terminal ligand on the apical position. This structure is represented by $Cu_2(COO)_4$ SBU.

The connection between the metal-containing SBUs via the carbon backbones of organic linkers forms porous crystalline structures of MOFs.[22] The judicious use of appropriately shaped SBUs and rigid organic linkers results in the formation of pre-determined MOF topologies.[23,24] The well-known example is the design and preparation of MOF-5 framework.[25] In this framework, the zinc-carboxylate SBUs with six points of extension in octahedral geometries connect to phenyl rings of 1,4-benzenedicarboxylic (BDC) acids to form porous cubic structure (Figure 2.3).

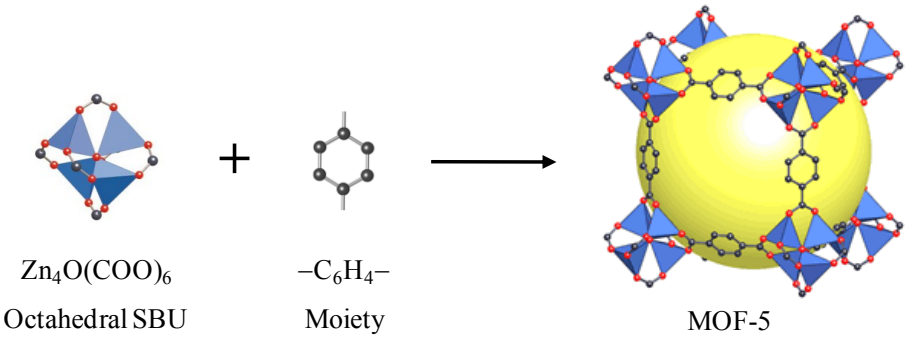

Figure 2.3 MOF-5 built from the connection of the octahedral SBUs with BDC acids. C: gray; O: red; Zn: blue tetrahedral. All hydrogen atoms are omitted for clarity. The large yellow sphere represents the largest van der Waals sphere that fits in the cavity of the framework. Reproduced with the permission of Nature Publishing Group.[25]

In principle, an almost unlimited number of MOFs can be constructed due to a great diversity of organic linkers and metal-containing SBUs. The connection of a specific SBU with different organic linkers and vice versa leads to MOF structures with different

topologies. The illustrative example is shown in Figure 2.4. The connection of trigonal prism SBUs with different organic linkers, either BDC acids as ditopic linker or 1,3,5-benzenetricarboxylic (BTC) acids as tritopic linker, creates the different topologies of MIL-88B and MIL-100 (MIL standing for Materials of the Institute Lavoisier).[26,27] In the other hand, the connection of the same tritopic BTC linkers with dicopper square paddle-wheel SBUs instead of trigonal prism SBUs results in HKUST-1 topology (HKUST standing for Hong Kong University of Science and Technology).[28] As a result, the features of the resulted frameworks such as pore structure, porosity, rigidity of the frameworks and physicochemical properties are also different.

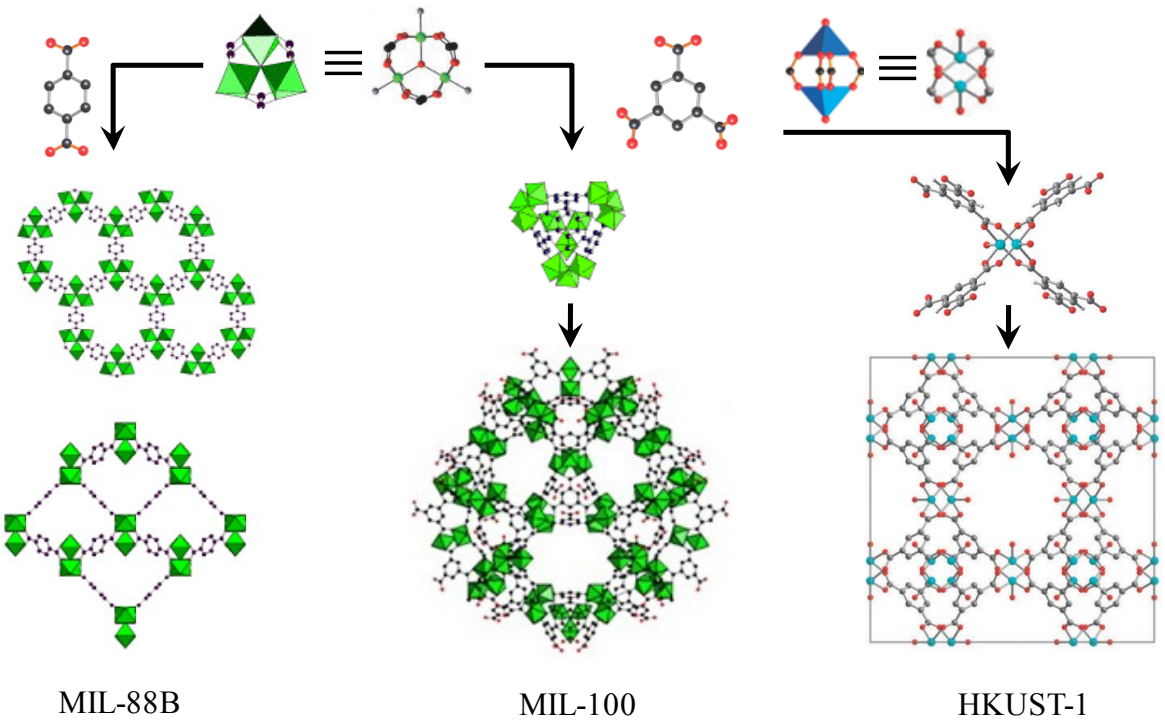

Figure 2.4 Topologies of MOFs from the different connections between SBUs and organic linkers. C: gray; O: red, Cu: cyan; metal such as Cr, Fe: green. Reproduced with the permission of The Royal Society of Chemistry, Willey and Elsevier.[26-28]

Functional groups such as $–NH_2$, $–NO_2$, $–SO_3H$, –CN, –OH, $–OC_xH_y$, $–C_xH_y$, $–CF_3$, –COOH, azide ($–N_3$) and halogens have been attached on organic linkers, commonly aromatic linkers, to generate functionalized MOFs.[29-38] The functionalized MOFs are often

monofunctional structures containing a single type of functional groups. The introduction of functional groups creates isoreticular MOFs with the same network, such as IRMOF-n (n = 2 – 5) possessing the network of IRMOF-1 (or MOF-5).[33] The functional groups can improve the stability and tailor the property of the parent structures for interesting applications. Multifunctional MOFs containing two or more distinct chemical functionalities have also been fabricated by integrating several organic linkers into a single platform.[39-41] The multifunctional MOFs provide integrated properties that their monofunctional counterparts can not achieve.[42]

MOF structures can be built from two or more types of organic linkers instead of one type of linker.[43-46] In the example to $[M_2(\text{dicarboxylate})_2(\text{N ligand})]_n$ MOFs, the three dimension structure of $[Cu_2(ndc)_2(dabco)]_n$ MOF is built from the connection of dicopper square paddle-wheel SBUs with two distinct linkers, including 1,4-naphthalene dicarboxylic (ndc) acid and 1,4-diaza-bicyclo[2.2.2]octane (dabco).[47] In this structure, NDC molecules connect with dicopper square paddle-wheel SBUs to form two dimension square lattices that are connected together by dabco molecules at the lattice points to form the porous structure (Figure 2.5).

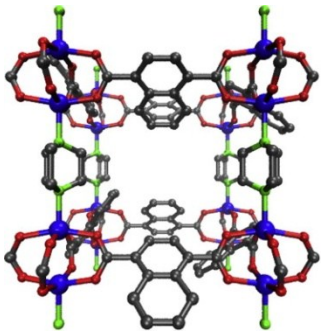

Figure 2.5 Structure of $[Cu_2(ndc)_2(dabco)]_n$. Cu: blue; N: green; O: red; and C: gray. All hydrogen atoms are omitted for clarity. Reproduced with the permission of Elsevier.[48]

The crystalline structures of MOFs are normally quite rigid. However, the reversible structural variation with retained topology can occur in various MOFs under external stimuli. Such variation of the flexible frameworks is usually called “breathing effect”.[49-51]

The breathing effect is activated by the presence of inserted guests such as water, solvents and gases. The breathing amplitude is governed by the host-guest interaction and the flexibility of MOF skeleton. The structural variation results in a dynamic change in the pore size and shape. During the breathing, the position of the Bragg peaks in the X-ray diffraction powder pattern shifts as a result of the change of the unit cell parameters.

The large breathing effect has been found in some carboxylate-based MOFs such as MIL-88 structures (MIL-88A constructed from fumaric acid, MIL-88B from BDC acid, MIL-88C from 2,6-naphthalenedicarboxylic (2,6-NDC) acid and MIL-88D from 4,4′-biphenyldicarboxylic (BPDC) acid),[27,52,53] MIL-53,[54-58] MIL-89,[59] DUT-8,[60] MCF-18,[61] and DMOF-1.[62,63] The possible breathing of a carboxylate-based MOF occurs only if structural rules are all satisfied.[49] The rules include the existence of a mirror plane in the SBU with the carboxylates in symmetrical positions toward them, for example in the square paddle-wheel dimers of DMOF-1 and the trigonal prism trimers of MIL-88; ditopic linker; and the absence of rigid odd cycles. Therefore, at variance to MIL-88, MIL-53 and DMOF-1; MIL-101 owning pentagonal windows,[64] MOF-5 consists of tetragonal SBUs without the mirror planes,[25] and HKUST-1 constructed from tritopic linkers[28] do not breath. Moreover, it seems that the ratio of number of carbons of the carboxylates surrounding the SBU to number of metal atoms within the SBU must be greater than or equal to 2 for such breathing effect.

In the illustrative example based on MIL-88B,[65] the topology has large cages with a trigonal bipyramid shape. The vertices of the bipyramid are occupied by trigonal prism SBUs. The ditopic linkers are on the edges of the bipyramid and there is no link in the equatorial plane of the bipyramind. The SBUs can rotate around the knee cap O–O axes of the carboxylates and the OOC–COO axes of the linkers (Figure 2.6, left). These rotations accompanying with the absence of rigid linkages between the equatorial SBUs can induce a change in the distance between the equatorial SBUs under external stimuli, leading to breathing effect. Indeed, the as-synthesized form of MIL-88B contains a few solvent molecules in the bipyramid cage. When the solvents are removed from the cage (dry form), the length between the two non-equatorial SBUs increases whereas the distance between

the equatorial SBUs decreases. In contrast, the bipyramid flattens and its volume increases if the solvents are exchanged into the cage (open form) (Figure 2.6, right). The expansion of the cell volume between the dry and open forms of MIL-88B can be over 125 %.

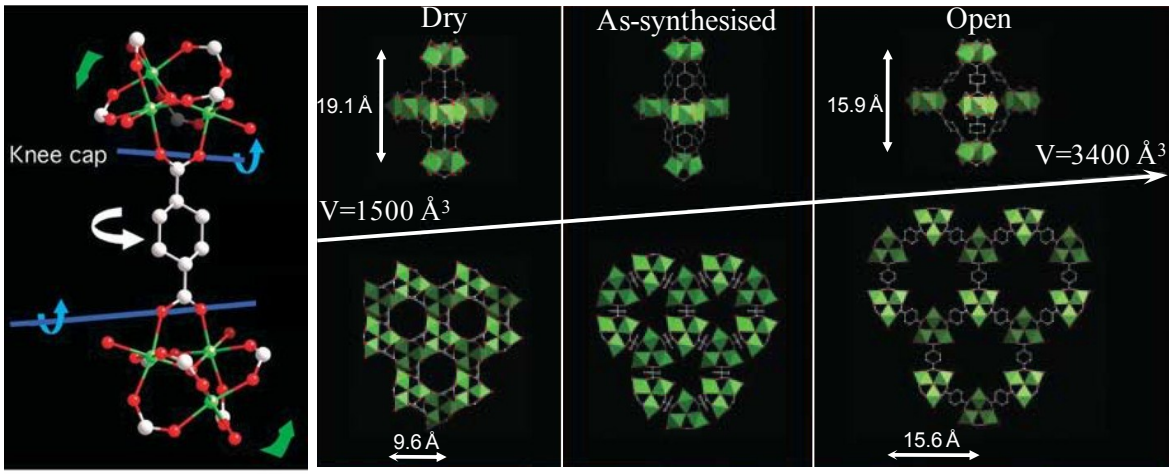

Figure 2.6 (Left) One edge of the trigonal bipyramid and the possibility of rotation around the knee cap O–O axes (blue lines) with the senses of the rotations (blue arrows) of the whole SBUs (green arrows) in MIL-88B. White arrow shows possible rotations around the OOC–COO axis of the linker. (Right) Evolution of the bipyramid (top) and correlative evolution of the structure along [001] (bottom) during breathing. Reproduced with the permission of Science and The Royal Society of Chemistry.[65]

The organic linkers and metal-containing SBUs impart the characteristics of MOFs such as high porosity with large surface area and pore volume,[66,67] high stability,[68] and the ability to tailor the pore cavity environment.[69,70] The extraordinary degree of variability for both organic linkers and metal-containing SBUs leads to tunable properties that make MOFs of interest for potential applications such as gas storage,[71-76] separation,[77-79] catalysis,[80-82] sensing,[83-86] biomedicine,[87-89] and proton conductivity.[90-94] Moreover, the post-synthetic modifications also allow the manipulation of the physical and chemical properties of a given MOF in a controllable manner.[69,95-99] Therefore, the design and use of organic linkers as well as the selection of metals focus on MOF structures suitable for their targeted applications.[6] For instance, the incorporation of electron-rich functional groups on the

organic linkers provides high affinity with CO_2 gas which promotes preferential CO_2 adsorption and separation,[34,100,101] while the attachment of achiral functionalities offers catalytic activity for enantioselective reactions.[81] Similarly, coordinatively unsaturated metal ions in square paddle-wheel or trigonal prism SBUs after the removal of axial terminal ligands act as Lewis acid sites that have high affinity with various guests such as adsorbates,[102-104] catalytic organic molecules,[105,106] porosity-customizing agents,[107] and reagents generating proton conductivity.[108] A number of MOFs built from lanthanide metals have luminescence that makes them ideal for sensing,[109,110] while various MOFs constructed from paramagnetic metals have magnetism suitable for magnetic applications.[111-113]

2.2 Mesoporous metal-organic frameworks

One of the most important properties of MOFs is porosity with large surface area and high pore volume. The IUPAC classifies porous solids into three categories according to their pore size: microporous ($d < 2$ nm), mesoporous ($2\ nm \leq d \leq 50$ nm) and macroporous ($d > 50$ nm) materials. Therefore, most of the reported porous MOFs are microporous and only a small fraction of MOFs are mesoporous (Table 2.1). The concept of the mesoporous MOFs refers not only to structures possessing large cavities and/or channels with diameters over 2 nm but also to MOF particles owning mesopore systems derived from supramolecular templates which are similar to those of conventional mesoporous materials.

2.2.1 MOFs with mesocages

A number of MOFs having large cavities within the range of 2 – 50 nm (so-called mesocages) have been prepared from one type of organic linker or the mixture of different linkers in coordination with metal-containing SBUs that possess different geometric shapes. One of these MOF structures is MIL-101.[64] The structure of MIL-101 consists of trigonal prism SBUs and ditopic linkers. The connection between the SBUs and the ditopic BDC linkers constructs microporous super tetrahedron (ST) (Figure 2.7). The four vertices of the ST are occupied by the SBUs while the ditopic linkers locate at the six edges of the ST. The

STs are computationally assembled through their vertices to produce an open framework with the Mobil thirty-nine (MTN) zeotype topology. In this assembly, the STs serve as tetrahedral TO_4 units of the MTN zeotype. MIL-101 structure has two types of mesocages with internal diameters of 29 Å and 34 Å. The small mesocage constructed by 20 STs has 12 pentagonal windows while the large mesocage defined by 28 STs has 12 pentagonal and 4 hexagonal windows. Although these cages are mesopores, the apertures of the windows in MIL-101 are limited within the size range of micropore at 12 Å for the pentagonal windows and 14.7 × 16 Å for the hexagonal windows.

The extension of the length of the ditopic linker creates larger mesocages within MIL-101 structure. Ferey *et al.* used 2,6-NDC acid that has a longer carbon backbone rather than that of BDC acid for the preparation of MIL-101_NDC material.[114] Similar to MIL-101 based on BDC acid, MIL-101_NDC is also constructed from ST subunits and has the MTN zeotype structure. However, the ST of MIL-101_NDC material (about 10.2 Å) is larger than that of MIL-101 (about 8.6 Å) because of the longer carbon backbone of 2,6-NDC acid. This results in two larger mesocages of MIL-101_NDC with internal diameters of 39 Å and 46 Å. The pentagonal and hexagonal windows have free diameters of approximately 13.5 Å and 18.2 × 20.3 Å, respectively.

Table 2.1 The structural features of representative mesoporous MOFs.

MOFs	Linkers	Mesoporous structure (Å)			Apertures (Å)	Ref.
		Cages	Channels	Templates		
MIL-101	BDC	29 and 34			12.0 and 14.7	[64]
MIL-101_NDC	2,6-NDC	39 and 46			13.5 and 18.2	[114]
MIL-100	BTC	25 and 29			4.8 and 8.6	[26]
Tb-mesoMOF	TATB	39 and 47			13.0 and 17.0	[115]
UMCM-2	T_2DC and BTB	26 × 32				[116]
DUT-6/MOF-205	NDC and BTB	25–30				[117, 66]
MOF-210	BTE and BPDC	26.9 × 48.3				[66]
PCN-53	BTTC	22.2			16	[118]
PCN-68	PTEI	23.2				[119]
PCN-610/NU-100	TTEI	27				[119, 120]
NOTT-119	H_6L	~25			19	[121]
ZIF-95	cbIM	~24			3.65	[122]
ZIF-100	cbIM	35.6			3.35	[122]

Table 2.1 (Continuous)

MOFs	Linkers	Mesoporous structure (Å)			Apertures (Å)	Ref.
		Cages	Channels	Templates		
Bio-MOF-1	Adenine and BPDC	mesocage	28 (3-D)			67
IRMOF-16	TPDC		28.8 (3-D)			33
mesoMOF-1	TATAB		22.5 × 26.1 (3-D)			123
CYCU-3	SDC		28.3 × 31.1 (1-D)			124
JUC-48	BPDC		21.1 × 24.9 (1-D)			125
IRMOF-74	DOT		14 – 98 (1-D)			126
PCN-222	TCPP		37 (1-D)			127
UMCM-1	BTB and BDC		27 × 32 (1-D)			128
MMOF-n	Disulfonate		61 – 75	F127		129
Zn-BDC	BDC		30	N-EtFOSA		130
$Cu_3(BTC)_2$	BTC		25	N-EtFOSA		131
$Cu_3(BTC)_2$	BTC		38 – 310	CTAB/TMB		132
MOF-5	BDC		> 100	DBA		133

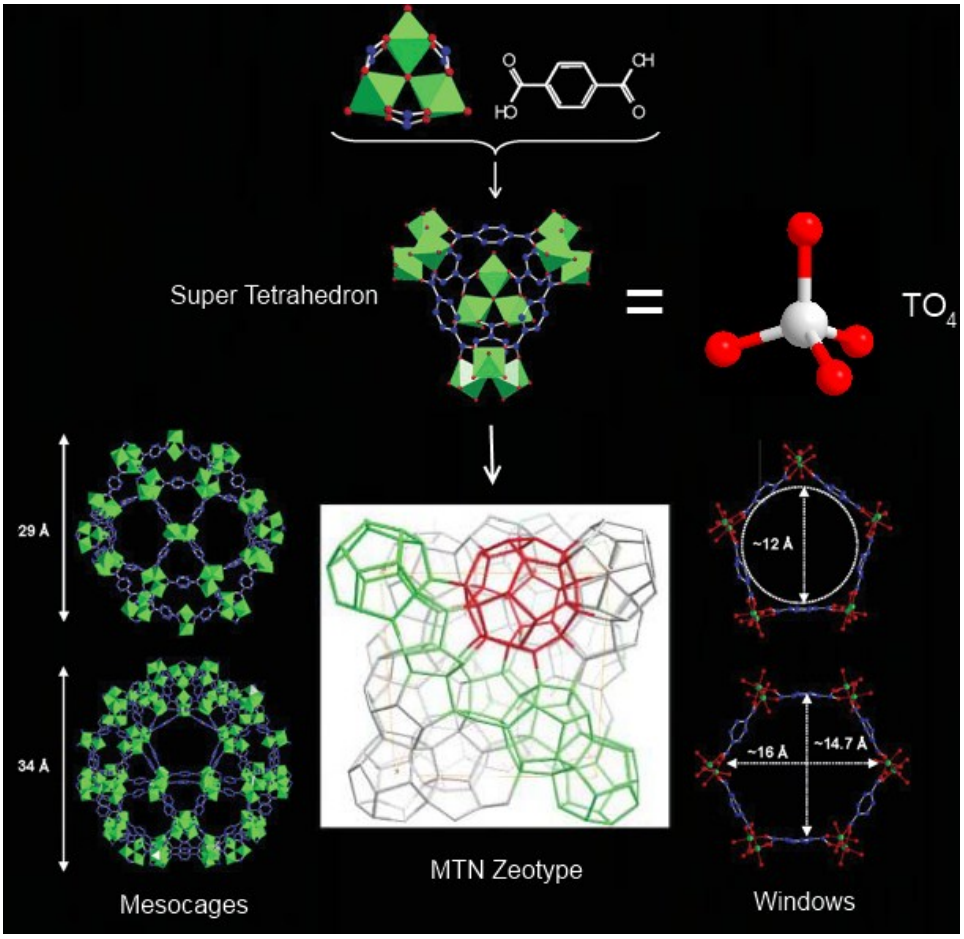

Figure 2.7 Architecture of the mesocages and windows in MIL-101. In the scheme of the MTN zeotype structure, the small and large mesocages are presented in green and red, respectively. Metal octahedral: green; O: red; C: blue. Reproduced with the permission of Science.[64]

By using tritopic BTC linker instead of ditopic BDC linker in coordination with the trigonal prism SBU, mesoporous MIL-100 with the same MTN zeotype topology was previously prepared by Ferey *et al*. in 2004.[26] The structure of MIL-100 is also constructed from tetrahedral ST subunits, in which four BTC linkers span four faces of the ST while the vertices of the ST are still occupied by the trigonal prism SBUs (Figure 2.4). Each BTC connects three trigonal prism SBUs via its three carboxylate groups and the phenyl ring of BTC occupies the center of the triangle face obtained by joining the three SBUs. Therefore, the ST in MIL-100 has smaller diameter rather than its counterpart in MIL-101, at 6.6 Å

and 8.6 Å, respectively. As a result, the mesocages of MIL-100 have smaller diameters at 25 Å for the small cage and 29 Å for the large cage. Similar to MIL-101 material, the windows of MIL-100 have small diameters at 4.8 × 5.8 Å for the pentagonal windows and 8.6 × 8.6 Å for the hexagonal windows.

Using a longer tritopic linker, 4,4′,4″-s-trizaine-2,4,6-triyltribenzoic acid (TATB), Kim *et al.* prepared a mesoporous MOF from Tb^{3+} ions (namely Tb-mesoMOF) possessing the same MTN zeotype topology as that of MIL-100 and MIL-101.[115] In this case, the tritopic TATB linkers connect trigonal-planar Tb_4 clusters to produce STs (Figure 2.8). Each face of the ST is spanned by the pair of TATB linkers that stack with each other. The outer TATB of this pair joins three peripheral Tb^{3+} ions in a bidentate fashion while the inner TATB links three central Tb^{3+} ions and other three peripheral Tb^{3+} ions in a bi-monodentate fashion. Because the carbon backbone of TATB is elongated by three additional phenyl rings when compared to that of BTC and BDC, the mesocages in Tb-mesoMOF are larger than those of MIL-100 and MIL-101 as the result of the increase in the dimension of the STs. The internal diameters of the mesocages are 39 Å and 47 Å. Although the mesocages are larger, the apertures of the windows are also limited within micropore regime at 13 Å for five-membered rings and 17 Å for six-membered rings.

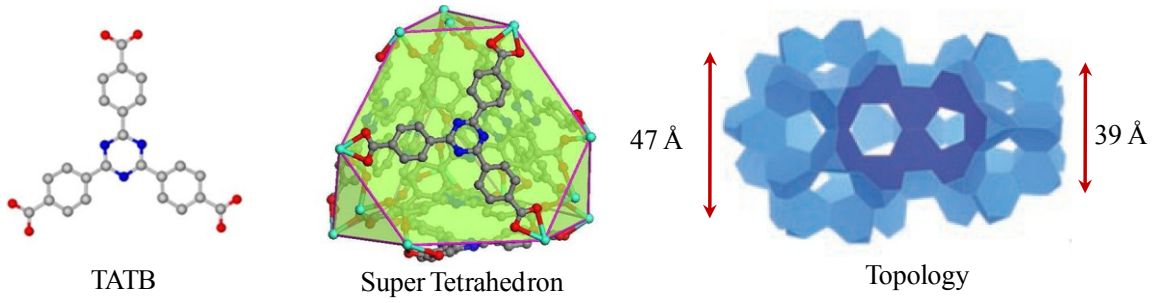

Figure 2.8 The ST consisting of TATB acids and trigonal-planar Tb_4 clusters and the topology of Tb-mesoMOF. Each blue truncated tetrahedron on the topology represents one ST. C: gray; O: red; N: blue; Tb: turquoise. Reproduced with the permission of Wiley InterScience and American Chemical Society.[115]

Besides one type of linkers, some MOFs having mesocages are constructed from the mixture of different types of linkers. Indeed, the coordination of ditopic thieno[3,2-b]thiophene-2,5-dicarboxylate (T_2DC) and tritopic 1,3,5-tris(4-carboxyphenyl)benzene (BTB) with zinc in the form of octahedral $Zn_4O(COO)_6$ SBUs produces mesoporous UMCM-2 MOF (UMCM standing for University of Michigan Crystalline Material).[116] UMCM-2 structure has a mesocage with internal dimension of approximately 26 × 32 Å and two different microporous cages (Figure 2.9).

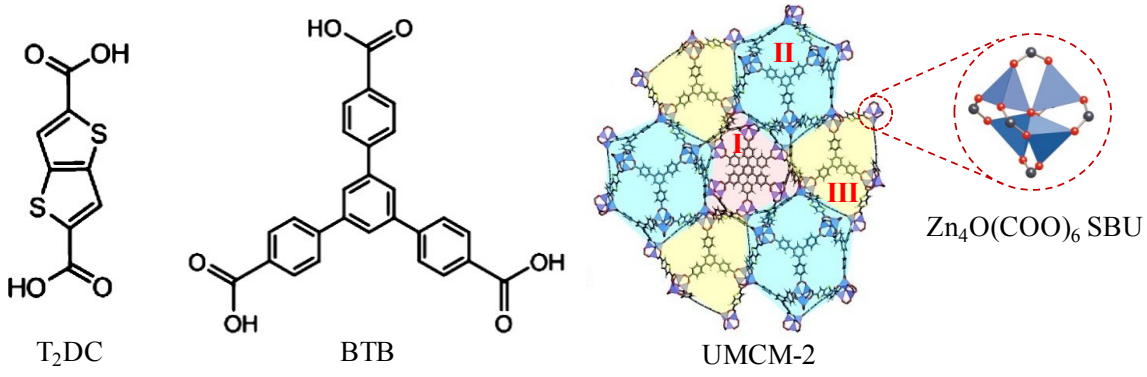

Figure 2.9 Structure of UMCM-2. The cage II (in cyan) is mesoporous while the cages I (in red) and case III (in yellow) are microporous. Reproduced with the permission of American Chemical Society.[116]

DUT-6 (DUT standing for Dresden University of Technology) with mesocages is also built from the mixture of ditopic 2,6-NDC linker and tritopic BTB linker which connect to octahedral $Zn_4O(COO)_6$ SBUs (Figure 2.10).[117] The carboxylate groups in the SBU come from four BTB linkers in a square planar arrangement and two 2,6-NDC linkers. The MOF structure provides dodecahedral mesocages with diameter of 25 – 30 Å which are built from twelve $Zn_4O(COO)_6$ SBUs, six 2,6-NDC linkers and eight BTB linkers. The second type of cage in DUT-6 is constructed from four $Zn_4O(COO)_6$ SBUs, two 2,6-NDC linkers and four BTB linkers. These smaller cages are arranged to connect the mesocages to form a periodic space filling. This MOF structure was independently reported as MOF-205 by Yaghi *et al.* in 2010.[66]

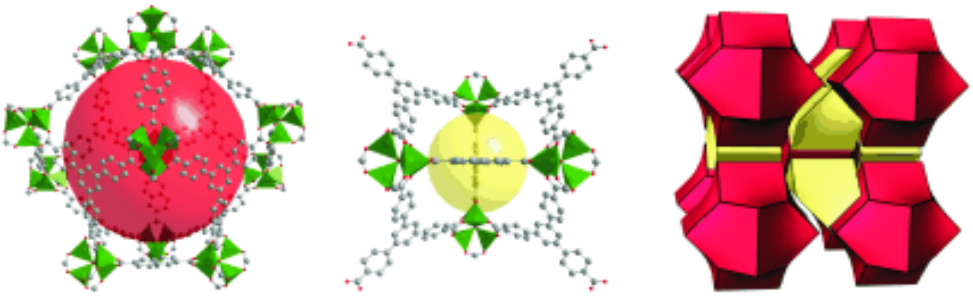

Figure 2.10 Structure of mesoporous DUT-6. Reproduced with the permission of Wiley InterScience.[117]

Recently, MOF-210 with mesocages has been prepared from the mixture of ditopic BPDC and tritopic 4,4′,4″-(benzene-1,3,5-triyl-tris(ethyne-2,1-diyl))tribenzoate (BTE) linkers (Figure 2.11).[66] The largest mesocage with a dimension of 26.9 × 48.3 Å in MOF-210 consists of eighteen $Zn_4O(COO)_6$ SBUs, fourteen BTE and six BPDC linkers. The material exhibits an enormous BET surface area of 6240 m^2g^{-1} and a total carbon dioxide storage capacity of 2870 $mg.g^{-1}$.

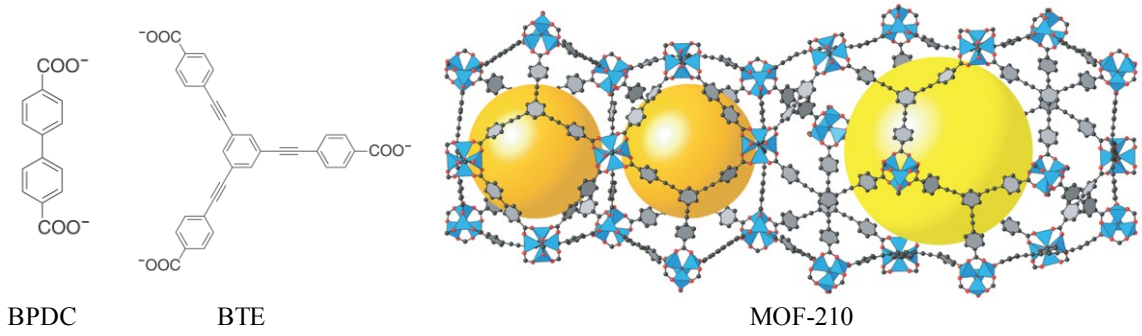

Figure 2.11 Structure of MOF-210. The yellow and orange spheres indicate spaces in the cages. Reproduced with the permission of Science.[66]

Although the MOFs possessing mesocages exhibit mesoporous features, their small apertures of the windows within the micropore range below 20 Å limit the access of large substances to the mesocages. The increase of the apertures to the mesopore range is still a great challenge.

2.2.2 MOFs with mesochannels

2.2.2.1 Three dimension mesochannels

The common strategy to enlarge the channels of MOFs toward the mesopore range of 2 – 50 nm (so-called mesochannels) is the extension of organic linkers. The linker extension takes the advantage of the increase of the channel size corresponding to the length of the linker. However, the linker expansion can result in catenated structures with small channels.[134] Moreover, MOFs built from long linkers can be collapsed upon guest removal.[135] Therefore, the construction of a MOF with 3D mesochannels from a given network topology via the extension of the linker should inhibit the catenation and collapse.[84,134]

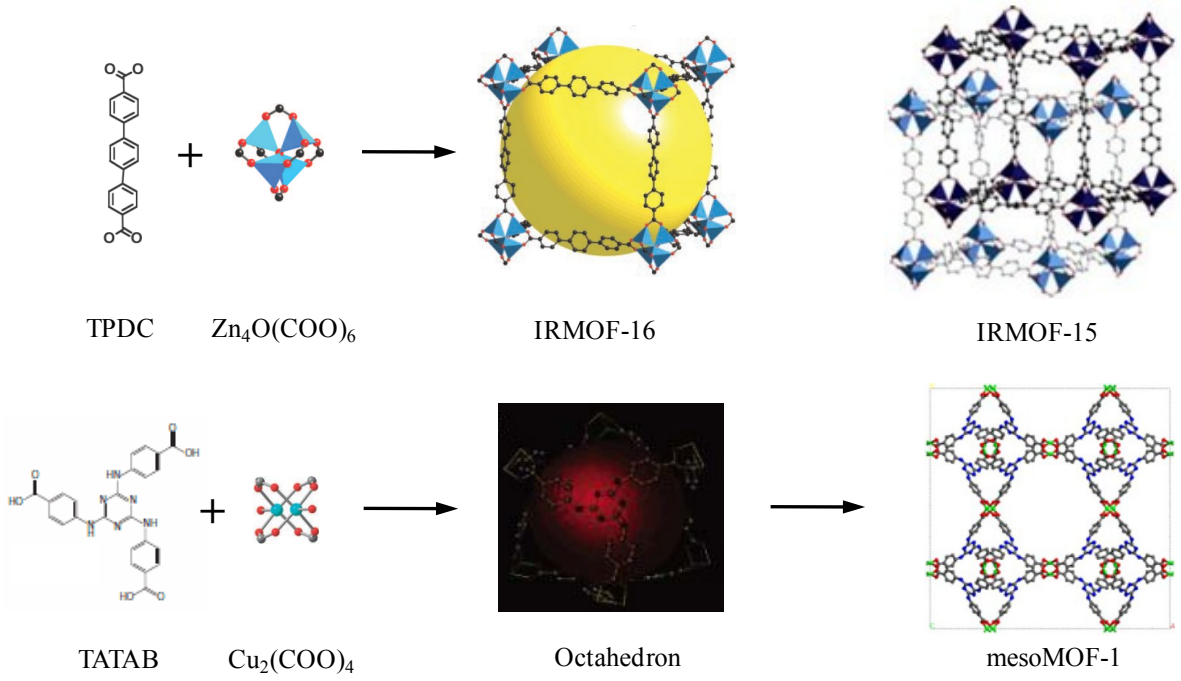

Figure 2.12 Structure of non-catenated IRMOF-16, interpenetrated IRMOF-15 isomer and mesoMOF-1. The colored spheres represent the void inside the cavities. Reproduced with the permission of Science, American Chemical Society and Elsevier.[33, 123]

The typical non-catenated MOF with 3D mesochannels prepared via the extension of linker is IRMOF-16.[33] The MOF has the same topology of MOF-5 (IRMOF-1), in which $Zn_4O(COO)_6$ octahedral SBUs connect to the aromatic backbones of ditopic carboxylate linkers to form cubic network (Figure 2.12, top). In MOF-5, the carbon backbone has one phenyl ring, giving micropores with the free- and fixed diameters of 11.2 Å and 18.5 Å, respectively. In contrast, the carbon backbone in IRMOF-16 is elongated with two additional phenyl rings, generating mesochannels with the free- and fixed diameters of 19.1 Å and 28.8 Å, respectively. IRMOF-16 should be synthesized under dilute conditions to avoid catenation that results in the interpenetrated structure of IRMOF-15 isomer with smaller micropores at 8.1 Å and 12.8 Å in free- and fixed diameters, respectively.

Zhou *et al.* prepared mesoMOF-1 with 3D mesochannels by the extention of tritopic carboxylate linkers.[123] MesoMOF-1 with the same topology of HKUST-1 is built from dicopper square paddle wheel SBUs and tritopic 4,4′,4″-s-triazine-1,3,5-triyltri-p-aminobenzoate (TATAB) linkers (Figure 2.12, bottom). Although TATAB has a longer carbon backbone rather than BTC in HKUST-1, mesoMOF-1 has non-interpenetrated structure because of the nonplanarity of TATAB linkers. In mesoMOF-1 structure, each $Cu_2(COO)_4$ SBU connects four TATAB linkers, and each TATAB links three SBUs to form an octahedron, in which all six vertices are occupied by the SBUs, and four of the eight faces are spanned by TATAB linkers. Eight such octahedra occupy the eight vertices of a cube to form a cuboctahedron through corner sharing. These cuboctahedra propagate to an open framework with 3D mesochannels of 22.5 × 26.1 Å in diameter.

Recently, An *et al.* have reported an alternative strategy for constructing mesoporous MOFs which addresses the size of the vertex rather than the length of organic linkers. They used large zinc-adeninate building units (ZABUs) as vertices to construct bio-MOF-100 (Figure 2.13).[67] In bio-MOF-100, each ZABU consists of eight Zn^{2+} cations interconnected by four adeninates and two μ–oxo groups. Monodentate BPDCs occupy the remaining coordination sites on each tetrahedral Zn^{2+} cation. The ZABU is connected to four adjacent ZABUs via twelve BPDC linkers to generate open structure with mesocages and 3D mesochannels with

a diameter of 28 Å along the axes. This MOF structure exhibits the largest pore volume reported to date, up to 4.3 cm^3g^{-1}.

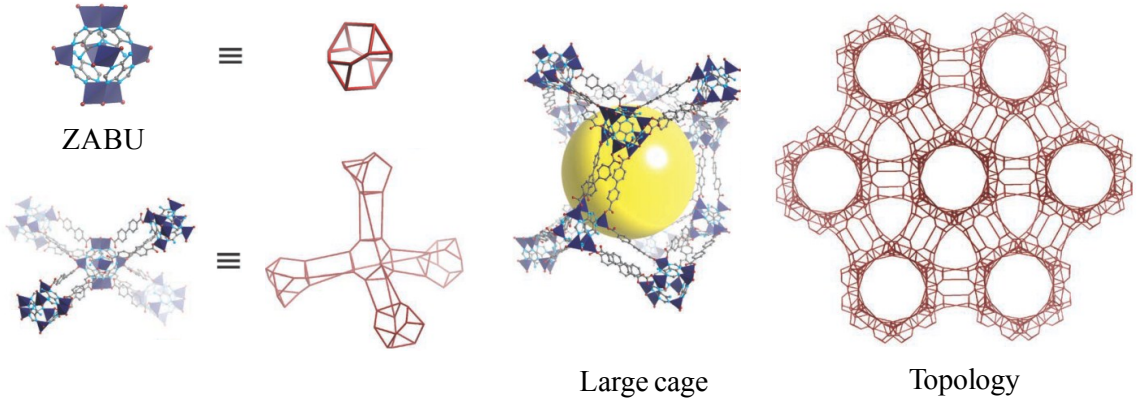

Figure 2.13 Structure of bio-MOF-100: ZABU can be treated as a distorted truncated tetrahedron. Each truncated tetrahedron connects four adjacent tetrahedra to generate open framework. Zn: dark blue tetrahedra; C: grey spheres; O: red spheres; N: blue spheres. Reproduced with the permission of Nature Publishing Group.[67]

2.2.2.2 One dimension channels

The construction of infinite rod-shaped SBUs has been employed to generate MOFs with 1D mesochannels such as CYCU-3 (CYCU standing for Chung-Yuan Christian University),[124] and JUC-48 (JUC standing for Jilin University China) materials (Figure 2.14).[125] In CYCU-3 structure, each octahedral Al^{3+} ion binds to four oxygen atoms from four carboxylate groups of 4,4'-stilbenedicarboxylic acids (SDC) and two oxygen atoms from the bridged hydroxide groups. The octahedral AlO_6 units form corner-shared 1D SBUs that are linked together by the SDC linkers to generate two types of 1D channels, including hexagonal mesochannels with the cross-section size of approximately 28.3 × 31.1 Å and triangular micropores with the pore size of 14.4 Å. Similarly, JUC-48 is constructed from rod-shaped Cd^{2+} carboxylate SBUs. These SBUs are interconnected through the biphenyl chains of BPDC linkers to generate a non-interpenetrated network with 1D hexagonal mesochannels of 24.5 × 27.9 Å.

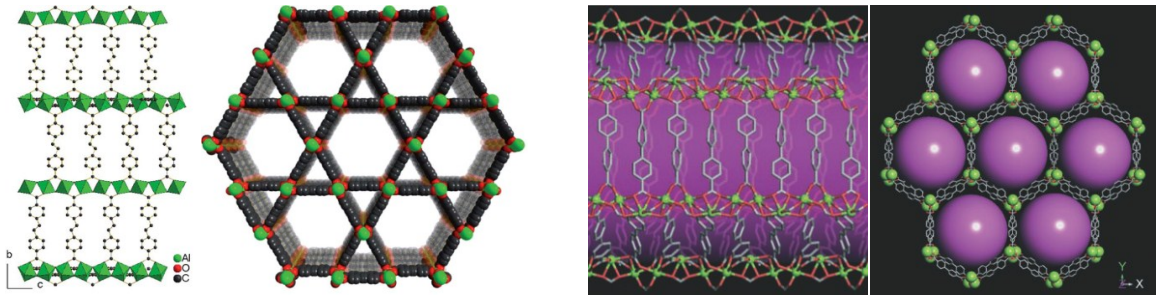

Figure 2.14 Structures of CYCU-3 and JUC-48. Reproduced with the permission of The Royal Society of Chemistry and Wiley InterScience.[124, 125]

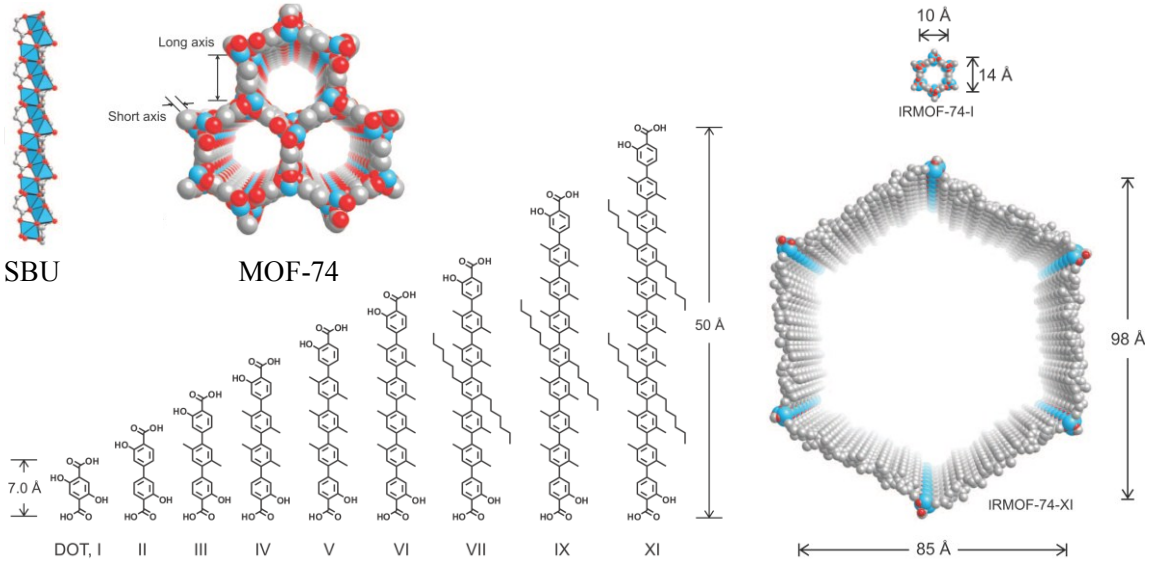

Figure 2.15 Structure of the series of nine IRMOF-74-I to XI. C: gray; O: red; metal: blue. Reproduced with the permission of Science.[126]

The construction of infinite rod-shaped SBUs in combination with the extension of organic linkers has been used for enlarging 1D channels of MOFs. The strategy has been employed for the systematic expansion of MOF-74 from its original link of one phenyl ring (I) (2,5-dioxidoterephthalate, DOT) to eleven (XI), which affords an isoreticular series of nine MOF-74 structures (termed IRMOF-74-I to XI) (Figure 2.15).[126] The topology of IRMOF-74 is built from infinite rod-shaped SBUs. The SBU is in a hexagonal arrangement joined

along the short and long axes by metal-oxygen bonds and organic DOT links, respectively. The formation of the short axis is ensured by the coordination of 5-coordinate metal atoms to the carboxylic and the ortho-positioned hydroxyl functionalities of DOT links. DOT links (long axes) join the infinite rod-shaped SBUs to make IRMOF-74 structure with 1D hexagonal channels. Upon the elongation of DOT links, the nine members of this series with non-interpenetrated robust structures have hexagonal channels in the range of 14 – 98 Å in size.

In a different assembly, the structure of PCN-222 (PCN standing for porous coordination network) containing 1D mesochannels is built from Zr_6 clusters instead of infinite rod-shaped SBUs (Figure 2.16).[127] In this structure, only eight edges of the Zr_6 octahedron are bridged by the carboxylates from square planar tetrakis(4-carboxyphenyl)porphyrin (TCPP) linkers, while the remaining positions are occupied by terminal hydroxy groups. Therefore, the framework of PCN-222 can be viewed as zirconium-carboxylate layers in the *ab* plane which are pillared by TCPP linkers along the *c* axis. PCN-222 provides 1D hexagonal mesochannels with a diameter of 37 Å. Moreover, the isomers of PCN-222 with uncoordinated porphyrin or metalloporphyrins including Fe, Mn, Co, Ni, Cu, and Zn can be produced, which affords a new series of PCN-222.

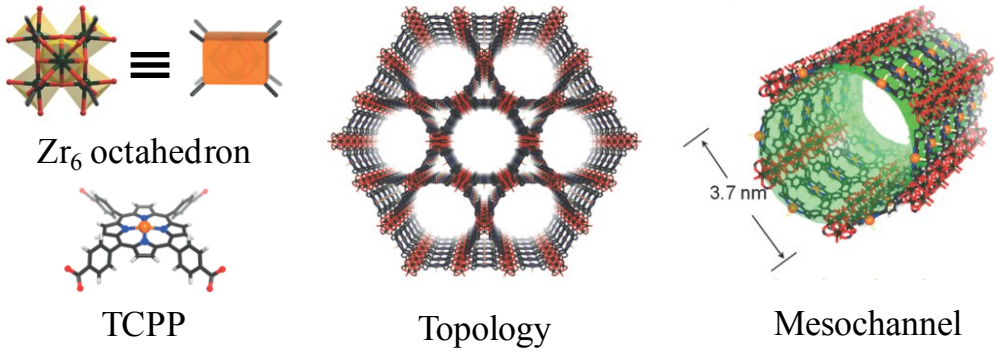

Figure 2.16 Structure of PCN-222. Zr: black; C: gray; O: red; N: blue; metal in porphyrin: orange. Reproduced with the permission of Wiley InterScience.[127]

The combination of different types of organic linkers has been employed for the construction of MOFs with 1D mesochannels. Koh *et al.* have synthesized mesoporous UMCM-1 by combining ditopic BDC with tritopic BTB in the presence of zinc cations (Figure 2.17).[128] Each octahedral Zn_4O SBU in UMCM-1 is coordinated by two BDC linkers and four BTB linkers. This structure generates micropous cages and 1D hexagonal mesochannels with a diameter of 27 × 32 Å.

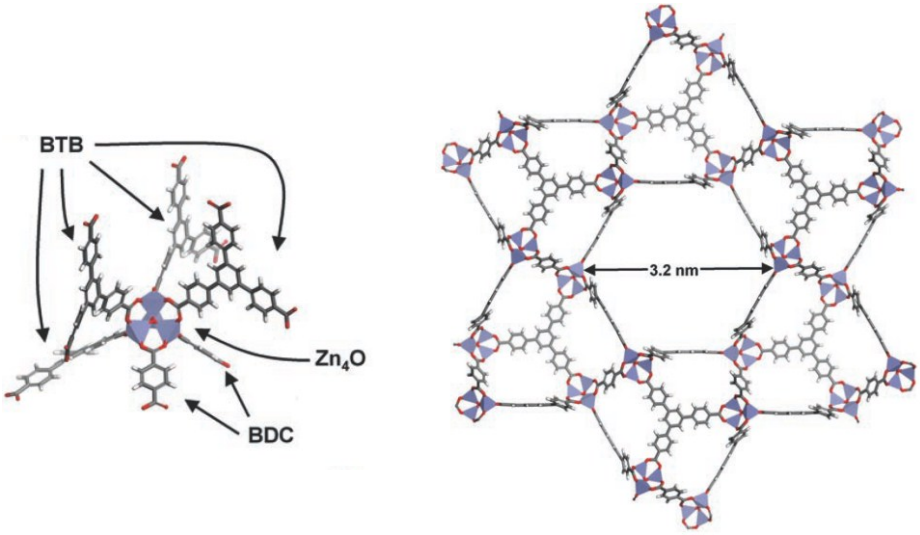

Figure 2.17 Structure of UMCM-1. Reproduced with the permission of Wiley InterScience.[128]

2.2.3 Mesoporous MOFs from supramolecular templates

The template-assisted synthetic approach has been adopted to prepare mesoporous MOFs. Similar to traditional mesoporous materials, the co-assembly approach uses structure-directing agents (supramolecular templates) for generating mesostructures (Figure 2.18). For the co-assembly into mesostructures and the growth of MOF directed by the templates, the interaction between MOF precursors and the supramolecular templates with considerable strength is essential. Otherwise, macroscopic phase segregation may take place, and the MOF will crystallize by itself despite the templates.[136]

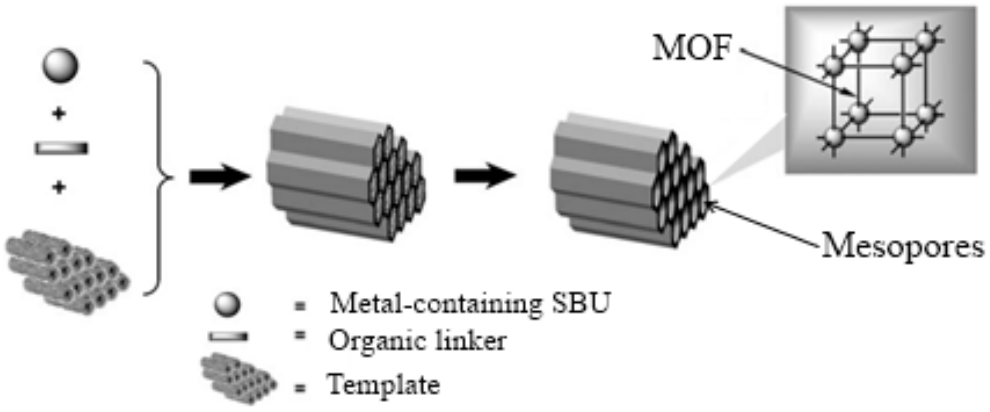

Figure 2.18 Schematic illustration of the synthesis of mesoporous MOFs using supramolecular templates. Reproduced with the permission of Wiley InterScience.[132]

2.2.3.1 Non-ionic templates

Nonionic triblock copolymers have been used as supramolecular templates for fabricating mesoporous MOFs. Ma *et al.* used the surfactant F127-induced co-assembly for producing MOFs with order mesopore structures from two disulfonic linkers (1,5-naphthalenedisulfonic and ethanedisulfonic acids) and different metal ions (Cd^{2+}, La^{3+}, Cu^{2+} and Sr^{2+}).[129] The MOF walls of the mesopores are built from the crystalline frameworks of metal-disulfonate. Since the easy coordination of the sulfonate groups with the metal ions facilitating the formation of large MOF crystals rather than the co-assembly between the surfactant and the MOF precursors into mesostructures, the crown ether 1,10-diaza-18-crown-6 was added to control the release of the metal ions, which slowed down the coordination rate between the metal centers and the sulfonate claws.

In such acidic synthesis system, the PEO segments of the triblock copolymer F127 (PEO–PPO–PEO) were protonated, producing positively charged head groups. The positively charged surfactants (S^oH^+), the disulfonate anions (X^-) and the metal cations (I^+) assembled together via $(S^oH^+)X^-I^+$ mechanism to form ordered hexagonal mesostructures. The propagation of the metal-disulfonate coordination (X^-I^+) formed the crystalline MOF walls of the mesostructures. After the removal of the F127 surfactant by acidic ethanol

extraction, the obtained MOF particles contained mesopores with the pore diameters in the range from 6.1 to 7.5 nm.

Nonionic N-ethyl perfluorooctylsulfonamide (N-EtFOSA) has also been used as supramolecular templates for synthesizing hierarchically micro- and mesoporous MOF particles. N-EtFOSA molecules self-assemble into cylindrical micelles, in which the fluorocarbon tails direct toward the inside of the micelles. By using N-EtFOSA, Zhao *et al.* synthesized MOF nanospheres with well-ordered hexagonal mesopores from Zn^{2+} ions and BDC acids in an IL/$SCCO_2$/surfactant emulsion system (IL = 1,1,3,3-tetramethylguanidinium acetate ionic liquid and $SCCO_2$ = supercritical CO_2).[130] Because of the strong interaction of the CO_2 molecules with the fluorocarbon tails, the CO_2 molecules existed as the core of the micelles. The coordination of Zn^{2+} ions with BDC linkers in the IL generated the microporous MOF walls. After the removal of the IL, CO_2, and the surfactant, uniform MOF nanospheres with well-ordered mesopores and microporous walls were achieved. The sizes of micropores, mesopores and the wall thickness were about 0.7, 3.0 and 2.5 nm, respectively.

Recently, Peng *et al.* have used N-EtFOSA as nonionic template for synthesizing mesoporous MOF nanoplates based on HKUST-1 structure in the IL solution.[131] In this case, the surfactant has a dual role in the formation of the mesoporous MOF nanoplates. On the one hand, the surfactant molecules play the role of a template in the mesopore formation. On the other hand, the surfactant can selectively adsorb onto the crystallographic planes of the MOF, thus serving as a directing agent and kinetically controlling the anisotropic growth of the MOF. In the process, Cu^{2+} ions in the IL first react with the deprotonated BTC to form nanosized framework building blocks. The nanosized building blocks then assemble with N-EtFOSA molecules to form mesostructured MOF particles. The removal of the surfactant from the mesostructured particles gives mesopores with the diameter around 2.5 nm.

2.2.3.2 Cationic templates

In addition to nonionic surfactants, cationic surfactants have been used for synthesizing mesoporous MOFs. In 2008, Qiu *et al.* used cetyltrimethylammonium bromide (CTAB) as cationic template for preparing MOFs with disordered mesostructures from Cu^{2+} cations and BTC linkers.[132] Under the similar reaction conditions of the synthesis of HKUST-1 from Cu^{2+} cations and BTC linkers, the CTAB molecules self-assembled into micelles that directed the formation of the mesostructures. The walls of the mesostructures were constructed from nanosized HKUST-1 domains. After the removal of the template by solvent extraction, the mesopores with a diameter up to 5.6 nm were fabricated, resulting in hierarchically micro- and mesoporous MOFs, in which the mesopores were interconnected by the intrinsic micropores of HKUST-1 with the diameter of 8.6 Å. Furthermore, the hydrophobic swelling agent 1,3,5-trimethylbenzene (TMB) was added to elongate the mesopores via swelling CTAB micelles. The diameter of the mesopores can increase to 31 nm in the presence of TMB.

In the same synthetic system, Sun *et al.* used citric acid as chelating agent for establishing a bridging interaction between copper ions and CTAB templates, which ensured the co-assembly of the MOF precursors and the templates into mesostructures.[136] The chelating agents interacted simultaneously with the copper ions and the CTAB molecules through Coulombic attraction and coordination.

2.2.3.1 Anionic templates

Long-chain carboxylic acid 4-(dodecyloxy)benzoic (DBA) was used for the preparation of sponge and pomegranate MOF-5 with mesopores and macropores in the range of 10 – 100 nm (Figure 2.19).[133] In a different mechanism from other surfactant templates, DBA served a dual purpose of having a carboxylate group for binding to Zn^{2+} ions of the SBUs, and a long alkyl chain for space filling. In the nucleation and crystal growth of MOF-5, DBA molecules attached to the growing crystal using their carboxylate functionalities and

hampered the local crystal growth to make mesopores and macropores using the long alkyl chains. DBA molecules were removed from the crystals by solvent exchange.

When large amounts of DBA were available, the mesoporous and macroporous system permeated from the center to the surface of the crystals, producing spongeous MOF-5 (spng-MOF-5). With lesser amounts of DBA, the crystals were 'starved' of DBA at the midpoint during the crystal growth, giving pomegranate MOF-5 (pmg-MOF-5) with spongeous core and solid outer shell.

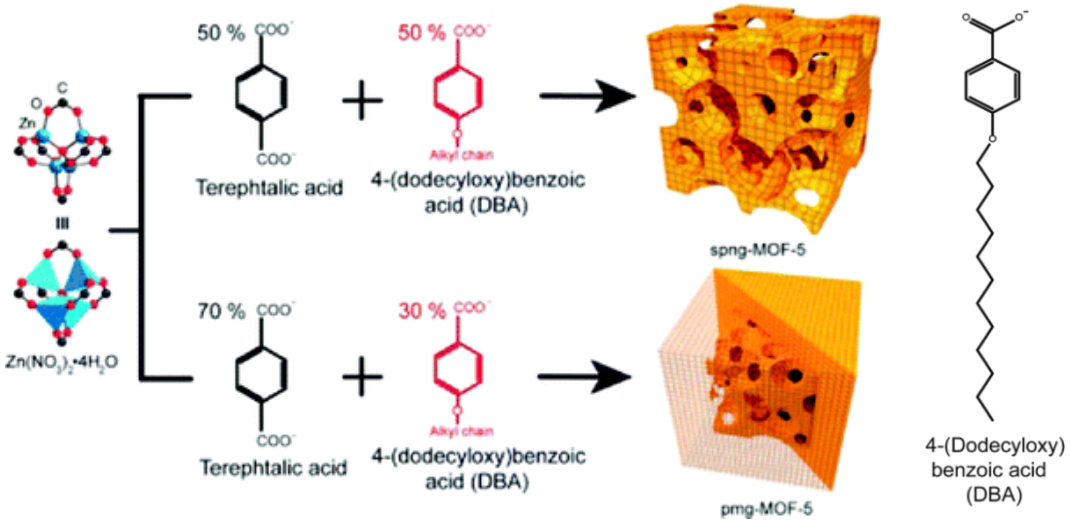

Figure 2.19 Schematic mesopore and macropore structures of spng-MOF-5 and pmg-MOF-5. Reproduced with the permission of American Chemical Society.[133]

2.2.4 Prospective applications of MOFs involving mesopores

In addition to the physicochemical properties involving organic linkers and metal-containing SBUs similar to those of microporous MOFs, mesoporous MOFs offer extensive features involving mesopores which are not exhibited by microporous MOFs. Combining the advantages of MOFs with the benefits of the mesopore networks, mesoporous MOFs can afford further applications such as in pharmaceutical field, enzymatic catalysis and the synthesis of nanoparticles.

2.2.4.1 Large molecule encapsulation

Mesoporous MOFs with wide pore apertures allow large and complex substances such as inorganic clusters, organic and biological molecules to access inside their pore systems. Yaghi *et al.* demonstrated that the pore apertures of IRMOF-74-IV to -IX were large enough for natural proteins and inorganic clusters to enter the mesopores, such as vitamin B_{12} with the largest size dimension of 27 Å in IRMOF-74-IV, myoglobin (globular protein) with spherical dimension of 21 × 35 × 44 Å in IRMOF-74-VII, GFP (barrel structure) with diameter of 34 Å and length of 45 Å in IRMOF-74-IX, and MOP-18 (inorganic spherical cluster) with diameter of 34 Å in IRMOF-74-V.[126] In another research, Yaghi *et al.* also indicated that the molecular dye rhodamine was preferably incorporated in the mesopores and macropores of spng- and pmg-MOF-5 rather than the micropores of MOF-5 because the diameter of rhodamine was much smaller than that of the meso- and macropores.[133]

Mesoporous MOFs have been employed as host matrix materials for heterogeneous biocatalysis.[137] Hierarchically porous MOFs contain mesopores as nanospaces to accommodate biocatalysts and micropores for the selective diffusion of reactants and products, resulting in shape or size-selective biocatalysis. Ma *et al.* reported the encapsulation of proteins, such as microperoxidase-11 with molecular dimension of about 3.3 × 1.7 × 1.1 nm,[138] cytochrome *c* with molecular dimension of about 2.6 × 3.2 × 3.3 nm,[139] and myoglobin with molecular dimension of about 2.1 × 3.5 × 4.4 nm,[140] in hierarchically microporous and mesoporous Tb-mesoMOF. Since the pore apertures of Tb-mesoMOF with diameters of 1.3 nm and 1.7 nm are smaller than the protein molecules, the proteins must undergo a change in conformation that is initiated by the surface contacts between the proteins and Tb-mesoMOF crystals to migrate through these small apertures into the mesocages (3.9 nm and 4.7 nm in diameter).[139] While microperoxidase-11 encapsulated in Tb-mesoMOF exhibited superior enzymatic catalysis toward the oxidation of 3,5-di-*t*-butyl-catechol to o-quinone by hydrogen peroxide, myoglobin squeezed into Tb-mesoMOF showed superior catalytic activities toward the size-selective oxidation of 2,2′-azinobis(3-ethyl-benzthiazoline)-6-sulfonate and pyrogallol by H_2O_2.

The functionalized walls of mesoporous MOFs can generate specific connections with complex organic molecules via post-synthetic modifications, leading to the possibility of tethering desired molecules onto the pore walls. Lui *et al.* employed strain-promoted "click" modification based on cyclooctyne derivatives for the incorporation of various functional groups onto the pore walls of azide-functionalized mesoporous bio-MOF-100 (*i.e.*, bio-MOF-100 built from 2-azidobiphenyldicarboxylic acids instead of BPDC acids).[141] The succinimidyl ester moieties of the functional groups allowed subsequent bioconjugation of biomolecules onto the pore walls. Therefore, this bioconjugation strategy can be used for tethering peptides, proteins (including enzymes), nucleic acids, polymers, dyes and nanoparticles onto the internal surface of mesoporous MOFs.

2.2.4.2 Confined nanospace synthesis

The mesocages of MOFs can act as nanoreactors where various chemical reactions can perform. A number of inorganic nanoparticles have been prepared in mesoporous MOFs without the collapse of the MOF structures. The size of the nanoparticles is restricted by the dimension of the mesocages. Because of the order arrangement of the mesocages, this restriction produces calibrated monodispersed nanoparticles on the MOF matrices. These impregnations can lead to significant changes in the textural properties of the MOFs such as adsorption capacity and catalytic activity.

In 2010, Ferey *et al.* prepared fluorinated inorganic clusters, $[(n\text{-}C_4H_9)_4N]_2[Mo_6Br_8F_6]$, in the mesocages of MIL-101 via a post-synthesis.[142] The inclusion of the fluorinated clusters in the mesocages improved hydrogen sorption of MIL-101 due to the interaction of terminal fluorine atoms with hydrogen molecules. Aluminium-based MIL-100 was also used as a host for synthesizing Pd nanoparticles with a size around 2.0 nm embedded within the mesocages without degradation of the porous host.[143] The H_2 uptake in the composite MIL-100/Pd was almost twice that of the pristine MIL-100 at room temperature.

Recently, ultrafine metallic Pt and bimetallic Au-Pd nanoparticles have been prepared in the mesocages of MIL-101 materials.[144] While the metallic Pt-immobilized MIL-101

nanocatalyst showed high catalytic activities in all three phases, including liquid-phase ammonia borane hydrolysis, solid-phase ammonia borane thermal dehydrogenation and gas-phase CO oxidation, the bimetallic Au-Pd-immobilized MOF nanocatalyst showed high catalytic activity for the generation of hydrogen from formic acid. Ni nanoparticles with a diameter up to 1.9 nm were also embedded in the mesocages of mesoMOF-1 by gas-phase loading of nickelocene and subsequent reduction.[145] These Ni-embedding mesoMOF-1 materials acted as catalysts for the hydrogenolysis of nitrobenzene to aniline or the hydrogenation of styrene to ethylbenzene.

In addition to metallic and bimetallic nanocatalysts, polyoxometalates such as polyoxotungstates $[PW_4O_{24}]^{3-}$ and $[PW_{12}O_{40}]^{3-}$ were fabricated into the mesocages of the MIL-101 for catalyses.[146,147] The hybrid polyoxotungstates/MIL-101 materials behaved as true heterogeneous catalysts for H_2O_2-based alkene epoxidation.

2.3 Nanosized metal-organic frameworks

Various strategies have been developed to miniature the size of MOF crystals to the nanometer scale, which offers a host of intriguing properties distinguishing from those of the bulk counterparts. A number of MOF morphologies with zero-dimensional (e.g., nanocubes), one-dimensional (e.g., nanowires, nanorods), two-dimensional (e.g., nanoplates, nanosheets) and anisotopic nanostructures have been fabricated. In general, bottom-up technique using atomic or molecular precursors has been used extensively because the morphology of MOF nanocrystals can be precisely controlled. In this technique, capping reagents, stabilizing reagents, microemulsions and the variations in synthetic parameters have been employed for the productions of nanosized MOFs. Recently, top-down technique using bulk MOF precursors has been adopted to prepare nanosized MOFs.

2.3.1 Coordination modulation

Coordination modulation approach uses capping reagents (termed modulators) for inhibiting the growth of MOF nanoparticles by coordinatively bonding to the surface-exposed metal sites (Figure 2.20).[148] The modulator has a single functional group similar to that of the multitopic organic linkers. During the nucleation and crystal growth of MOFs, the modulators compete with the organic linkers in order to coordinate with the metal sites. The competition impedes the coordination interaction between the metal ions and the linkers which favors the formation of MOF nanocrystals. Furthermore, the selective coordination modulation can change the rate of framework extensions in different directions, resulting in controllable morphologies of MOF nanocrystals.

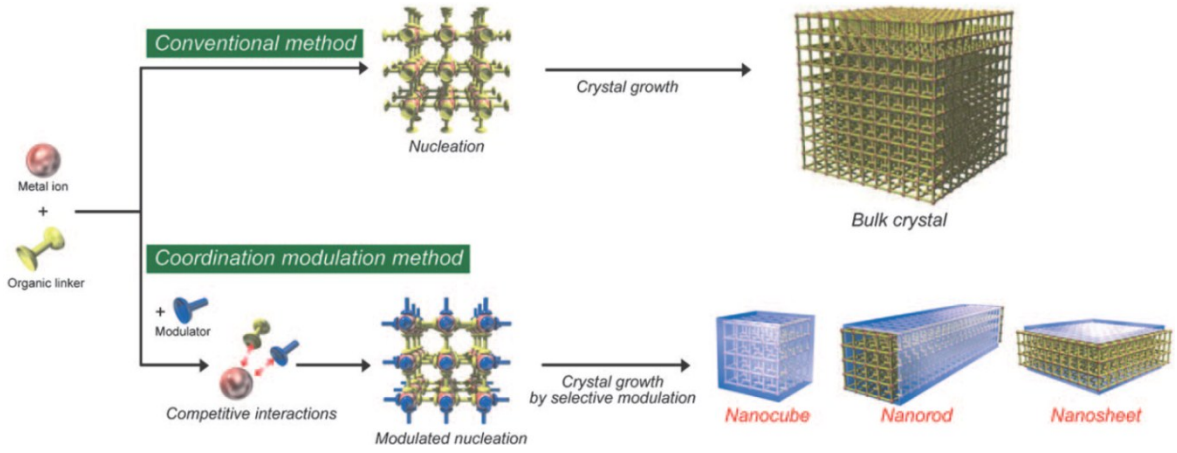

Figure 2.20 Coordination modulation approach toward MOF nanocrystals with different morphologies. Reproduced with the permission of Wiley InterScience.[148]

Monocarboxylic acids and their salts are commonly used as modulators for fabricating carboxylate-based MOF nanocrystals. The possibility to terminate the crystal growth of MOF nanoparticles by coordination modulation was first demonstrated by Fischer *et al.*, in which p-perfluoroethylbenzoic acid (pfmbc) was used as modulator for yielding MOF-5 nanoparticles.[149] In the growth solution of MOF-5, pfmbc modulator competed with BDC linker for coordination to the vacant edges of surface-exposed Zn_4O sites of MOF-5

colloids, yielding stable MOF-5 nanocrystals. The size of MOF-5 nanocrystals was changed in the range of 100 – 200 nm by adjusting the ratio of BDC and pfmbc.

Kitagawa *et al.* showed that the selective coordination modulation in one of coordination modes constructing MOF structure led to anisotropic growth of the MOF nanocrystals.[148] In three-dimensional pillared-layered $[Cu_2(ndc)_2(dabco)_n]$ structure as a model, the ndc linkers bind to dicopper square paddle wheel SBUs to form two-dimensional square lattices that are connected by pillar dabco linkers at the lattice points in the [001] direction. This assembly yields anisotropic framework dominated by two coordination modes, including copper-carboxylate and copper-amine. This allows the selective modulation of the copper-carboxylate modes by monocarboxylic acid. In the presence of acetic acid as modulator, the coordination interaction between copper and ndc was impeded because both ndc and acetic acid had the same carboxylic functionality, while the coordination of copper with dabco was not affected. Therefore, the selective modulation enhanced the relative crystal growth in the [001] direction, leading to the formation of the square nanorods. The length and thickness of the nanorods were adjusted by acetic acid concentration, in which the length corresponding to the copper-amine coordination directions increased whereas the width corresponding to the copper-carboxylate coordination directions decreased with an increase in the concentration of acetic acid.

Recently, Kitagawa *et al.* have also used acetic acid as modulator for preparing the nanoplates of twofold interpenetrated $[Cu_2(bdc)_2(bpy)]_n$ MOF.[150] The interpenetrated structure is composed of two identical but distinct frameworks that base on dicopper square paddle wheel SBUs interconnected with bdc in the equatorial plane and bpy in the apical positions. Each distinct framework is similar to $[Cu_2(ndc)_2(dabco)_n]$ framework in which bdc and bpy linkers are used in lieu of ndc and dabco, respectively. $[Cu_2(bdc)_2(bpy)]_n$ microcrystals were synthesized by first forming 2D square grids of $[Cu_2(bdc)_2(solvent)_2]_n$ from the reaction of copper ions and bdc acids. The coordination of bpy linkers to the dicopper SBUs of the square grids via the exchange reaction with the solvent molecules formed the bulk 3D framework. By adding acetic acid to the mixture of copper acetate and bdc in the first step of the synthesis, the square-like nanoplates were yielded. The width and

thickness of the nanoplates increased with an increase in the modulator concentration. Compared with the synthesis of $[Cu_2(ndc)_2(dabco)_n]$ nanorods, the modulator here had the opposite effect on the width corresponding to the copper-carboxylate coordination directions.

Monocarboxylate salts were used as modulators for synthesizing nanosized MOFs built from lanthanide cations (Ln = Dy^{3+}, Eu^{3+}, or Tb^{3+}) and BTC acid.[151] In the absence of the modulators, [Ln(BTC)(H_2O)] MOFs had rod-shaped microcrystals with a length of ~60 μm. While the addition of sodium formate as modulator resulted in fairly uniform bean-shaped nanocrystals with a length of ~125 nm and a width of ~100 nm, the presence of sodium acetate yielded smaller nanocrystals with a length of ~90 nm and a width of ~75 nm.

2.3.2 Stabilizing reagent

Stabilizing reagents suppress the crystal growth of MOF nanoparticles by adsorbing on the growing facets. The adsorption slows down the crystal growth rate of all the growing facets, which facilitates systematically the formation of the nanocrystals. The deceleration of the crystal growth rate depends on the adsorbance of the growing facets. Therefore, the relative crystal growth rates can be manipulated by using variable amounts of stabilizing reagents, resulting in the different morphologies of MOF nanocrystals. The appropriate stabilizing reagents are usually surfactants. In contrast to modulators, the stabilizing reagents can be removed from the surface of the resulted MOF nanocrystals.

Ma *et al.* synthesized MOF-5 nanocrystals by using a multi-step solvothemal process in the presence of CTAB surfactant as stabilizing reagent.[152] The surfactant was added to stabilize the incubated mother solution. The presence of CTAB thus slowed significantly the subsequent nucleation. After the nucleation, amines were added to accelerate the deprotonation of the linkers, resulting in the rapid growth of MOF-5 nanocrystals. In the incubated solution without CTAB, the fast uncontrolled-nucleation and crystal growth resulted in the microcrystals rather than the nanocrystals. Furthermore, the combination of CTAB with different amines (triethylamine, piperidine and decylamine) effected the

growth along different crystallographic axes, thereby allowing the formation of anisotropic nanoparticles. While decylamine with a long carbon chain induced the nanorods, triethylamine and piperidine induced the octahedral nanocrystals. After the synthesis, the CTAB surfactant was removed cleanly from the surface of MOF-5 nanocrystals by washing.

Xu *et al.* also demonstrated that the addition of different amounts of CTAB controlled the morphology of $Eu_2(FMA)_2(OX)(H_2O)_4{\cdot}4H_2O$ nanocrystals (FMA = fumarate, OX = oxalate).[153] They used the Bravais–Friedel–Donnay–Harker method for simulating the crystal growth and morphology control. In the absence of CTAB, the large rhombus truncated bipyramid microcrystals were fabricated. The gradual increase in CTAB amount in microemulsion system prepared the elongated hexagonal nanoplates and hexagonal nanoplates.

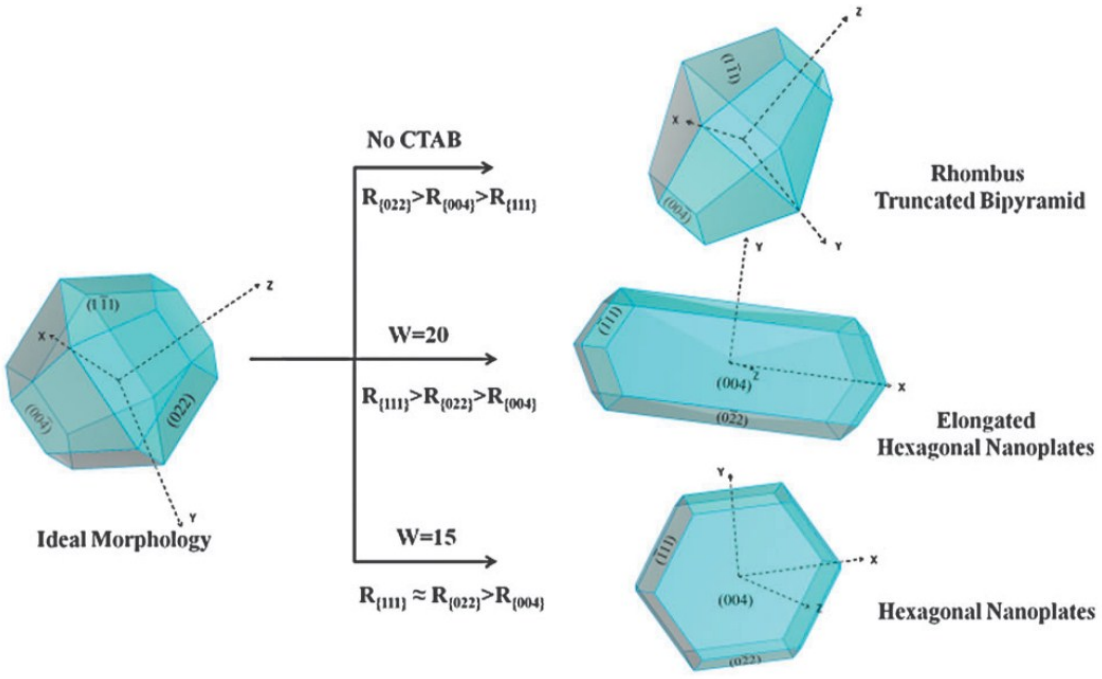

Figure 2.21 The morphologies of $Eu_2(FMA)_2(OX)(H_2O)_4{\cdot}4H_2O$ MOF simulated by modulating the growth rates of different growing facets. Reproduced with the permission of The Royal Society of Chemistry.[153]

The crystal structure of $Eu_2(FMA)_2(OX)(H_2O)_4 \cdot 4H_2O$ MOF has three possible growing facets {022}, {004} and {111} in which the growth rate R_{hkl} is in the order $R_{\{022\}} > R_{\{004\}} > R_{\{111\}}$ (Figure 2.21). In the absence of CTAB, the faster growing facet {022} tends to disappear, so the crystal morphology is dominated by {004} and {111} facets, leading to the formation of the large rhombus truncated bipyramid crystals. The addition of CTAB makes high surface energy facets {022} and {004} more thermodynamically favorable by preferential adsorption. Therefore, the crystal growth rate of {111} facet is faster than those of {022} and {004} facets, resulting in the elongated hexagonal nanoplates. When more CTAB is present, the crystal growth rate of {111} facets is also significantly prohibited, so $R_{\{111\}} \approx R_{\{022\}} > R_{\{004\}}$, leading to the formation of the hexagonal nanoplates.

The similar effect of CTAB surfactant on the morphology of nanoscale MOFs was observed for HKUST-1.[154] Since the growth rates of the growing facets were determined by the amount of CTAB, the morphological evolution of HKUST-1 nanoparticles from cube, to truncated cube, cuboctahedron, truncated octahedron, and to octahedron was occurred with an increase in the CTAB concentration. Furthermore, the presence of CTAB that slowed the nucleation rate led to an increase in the size of HKUST-1 crystals.

2.3.3 Microemulsion

Microemulsion is thermodynamically stable mixture of hydrophobic liquid, water and surfactant, frequently in the presence of co-surfactant such as short chain alcohols. In case water disperses in hydrophobic liquid, the mixture is called reverse microemulsion. In the reverse microemulsion, surfactant-stabilized aqueous nanodroplets are dispersed in hydrophobic organic phase. Such aqueous nanodroplets can act as nanoreactors for synthesizing MOF nanoparticles. In these synthetic processes, the precursors of MOFs are dissolved in the nanodroplets and the subsequent crystallization of MOF nanoparticles is induced by the collision between the nanodroplets or external stimuli. The size of the resulted MOF nanoparticles can be controlled via the control over the size of the nanodroplets by varying the molar ratio of water to surfactant (denoted as W).

The first example of the syntheses of nanosized MOFs in reverse microemulsions was reported in 2006.[155] The crystalline $Gd(BDC)_{1.5}(H_2O)_2$ nanorods and $Gd(1,2,4\text{-}BTC)(H_2O)_3$ nanoplates were prepared at room temperature in CTAB/1-hexanol/isooctane/water reverse microemulsions. The research demonstrated that the morphologies and sizes of the MOF nanoparticles were affected by the W value. Indeed, $Gd(BDC)_{1.5}(H_2O)_2$ nanorods of 100 – 125 nm in length by 40 nm in width were obtained with W = 5 while the larger rods of 1 – 2 μm in length and around 100 nm in width were obtained with W = 10.

The reverse microemulsion synthesis of nanosized MOFs at room temperature can generate amorphous particles due to the rapid coordination between metal ions and organic linkers. In these cases, the elevated temperatures favour the crystal growth of the crystalline MOF nanoparticles. Liu *et al.* indicated that the synthesis of nanosized MOFs from Gd and BHC at room temperature using reverse microemulsion only produced amorphous materials.[156] Therefore, the reverse microemulsion synthesis at high temperature was used for preparing crystalline $Gd_2(BHC)(H_2O)_6$ nanoparticles. The block-like nanocrystals with dimensions of 25 × 50 × 100 nm were prepared in CTAB/1-hexanol/n-heptane/water microemulsion (W = 10) after heating at 120 °C for 18 h.

By using the same CTAB/1-hexanol/n-heptane/water microemulsion, the rod-like $Mn(BDC)(H_2O)_2$ nanoparticles with diameter of 50 – 100 nm and length of 750 nm to several μm were obtained either at room temperature or under microware heating at 120 °C.[157] The crystalline $Mn_3(BTC)_2(H_2O)_6$ nanoparticles were also fabricated in the similar reverse microemulsion by using isooctane as continuous hydrophobic phase instead of n-heptane. The results indicated that the synthetic temperature impacted on the morphology of the $Mn_3(BTC)_2(H_2O)_6$ nanocrystals. While the spiral rod $Mn_3(BTC)_2(H_2O)_6$ nanoparticles with diameter of 50 – 100 nm and length of 1 – 2 μm were obtained at room temperature, the block-like nanocrystals with much lower aspect ratio and the length in the range of 50 – 300 nm were fabricated at 120 °C under microware heating.

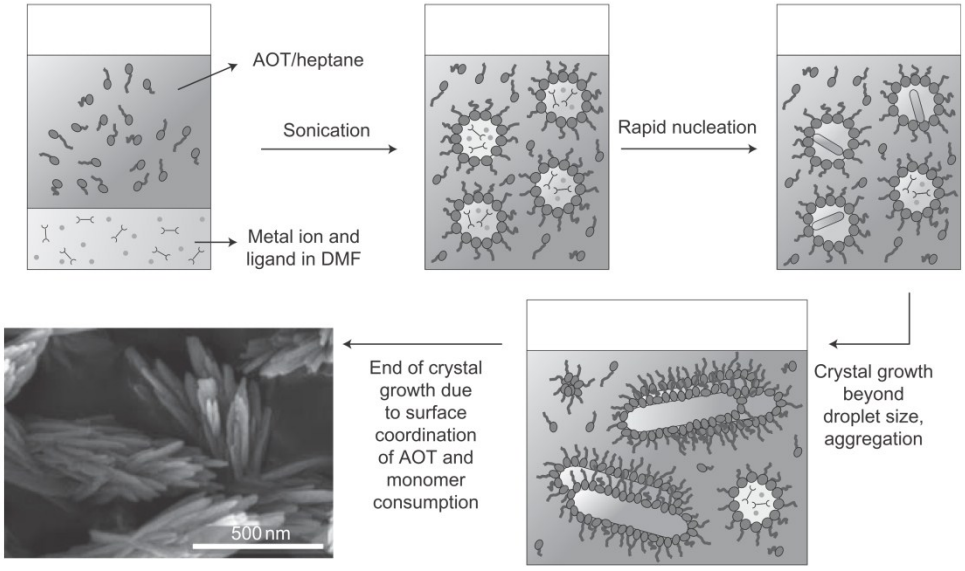

Figure 2.22 Model for the formation and growth of $[Zn(ip)(bpy)]_n$ nanorods in AOT/n-heptane/DMF reverse microemulsion. Reproduced with the permission of Nature Publishing Group.[158]

Because some organic linkers do not dissolve in aqueous phase, non-aqueous reverse microemulsions in which water is replaced by a polar organic solvent such as N,N-dimethylformamide (DMF) have been employed to synthesize MOF nanoparticles. Kitagawa *et al.* used non-aqueous AOT/n-heptane/DMF reverse microemulsion for the preparation of $[Zn(ip)(bpy)]_n$ nanocrystals at ambient temperature (AOT = dioctyl sulphosuccinate sodium).[158] Ultrasonic irradiation was required to induce the thermodynamically controlled crystallization of the MOF nanoparticles. The formation of the nanocrystals was accomplished within a few minutes. The crystalline nanorods with dimensions of 300 × 50 × 15 nm were obtained at W = 1. The increase in W value led to the larger nanorods. In contrast, the gel-like amorphous particles precipitated immediately in the AOT/n-heptane/DMF microemulsion system without sonication. The crystal growth of the nanorods was explained by the reversible formation of metal–linker bonds under high-energy irradiation in combination with constant merging of the nanodroplets (Figure 2.22). During the crystal growth, the particle size extended rapidly the nanodroplet size of the initial microemulsion, leading to an aggregation of the growing nanocrystals and the

surface coordination of AOT. Furthermore, the surface coordination of AOT also limited the diffusion of the metal ions and organic linkers to the crystal surface which limited the particle growth.

2.3.4 Synthetic parameters

The synthetic parameters including compositional parameters (metal source, reactant concentration, pH, solvent and molar ratio of reactants) and process parameters (time, temperature and heating source) can be adjusted to achieve MOF nanocrystals. However, there isn't general trend in variation of the synthetic parameters to generate MOF nanocrystals except microwave- and ultrasound-assisted syntheses. Therefore, the syntheses of nanosized MOFs by varying the synthetic parameters have to be fine-tuned for each system in a trial-and-error approach.

The syntheses under high-energy irradiation of microwave or ultrasound allow the fabrication of MOF nanocrystals in a short period of time.[159] In microwave-assisted synthesis, the high dielectric absorptivity of polar solvents results in a thermal conversion of high-energy microwave and thus efficient heating of reaction solution. The rapid and local heating leads to a fast and homogeneous nucleation. In case of ultrasonic-assisted synthesis, the cavitational collapse of the vacuum bubbles produced in the sonochemical reaction leads to very fast and intense local heating and high pressure, which allow both a rapid synthesis and a tuning of the kinetics of the reaction. The approaches are facile, rapid and environmentally friendly, but it is not easy to control the morphology and the size of the resulted nanocrystals.

Several MOF nanocrystals have been prepared by using microwave-assisted synthesis. MIL-101_NH_2 nanocrystals were prepared under microwave irradiation from an aqueous solution of 2-aminoterephthalic acid and $FeCl_3 \cdot 6H_2O$ at 60 °C for 5 min.[160] The resulted nanoparticles had an octahedral shape with diameter of 173 ± 60 nm. MIL-100 nanocrystals were similarly prepared from an aqueous mixture of iron powder, BTC and HF acid at 200 °C for 30 min. The resulted MIL-100 particles appeared as an aggregation of the smaller

spherical nanoparticles of 59 ± 46 nm rather than the individual nanocrystals. Through the systematic investigation into reaction conditions toward MIL-88A nanoparticles, Chalati *et al.* showed that hydrothermal microwave-assisted synthesis was a convenient and rapid route to obtain monodispersed MIL-88A nanoparticles with controllable size smaller than 100 nm.[159]

Ultrasonic-assisted method was applied to the synthesis of various nanosized MOFs such as $Zn_3(BTC)_2{\cdot}12H_2O$,[86] MOF-2,[85] $[Tb(btc)(H_2O)_6]_n$,[83] and HKUST-1.[161] The size and shape of the $Zn_3(BTC)_2{\cdot}12H_2O$ nanocrystals were strongly influenced by the irradiation time. The short period of reaction time in a few minutes produced the sphere-like nanoparticles of 50 – 100 nm in size. The irradiation up to 30 min prepared the wire-like nanoparticles with diameter of 100 – 200 nm and length of up to 100 mm. Further increase in reaction time increased the diameter of the wire-like crystals to 700 – 900 nm. The nanoparticles had a trend of aggregation rather than isolated nanocrystals. Nanobelts and nanosheets of MOF-2 were prepared under ultrasonic irradiation at ambient temperature. The nanobelts with a width of 150 – 300 nm and a length of 2 – 5 μm were obtained after 10 min irradiation. The nanosheets were formed with the reaction time up to 20 min. Further increase of the reaction time led to an increase in dimension of the nanosheets. Nanowires of $[Tb(btc)(H_2O)_6]_n$ with an average diameter of 50 nm and length of up to a few micrometers were produced under ultrasound irradiation at 70 °C and atmospheric pressure. HKUST-1 nanocrystals were fabricated by ultrasonic-assisted synthesis at ambient temperature and atmospheric pressure for short reaction times. The resulted HKUST-1 nanocrystals had a very wide range of particle size distribution.

The reaction temperature affects on the rate of nucleation and crystal growth, resulting in an impact on the shape and size of MOF crystals. MIL-88A with several crystal sizes was synthesized under hydrothermal conditions by varying the reaction temperature in the range of 65 – 150 °C.[159] The bar-like nanocrystals with a length of 250 ± 55 nm were obtained at 65 °C. The increase in the reaction temperature led to an increase in the crystal size. The synthesis at 150 °C produced the submicro-crystals of MIL-88A with a length of above 1.2 μm.

The synthetic processess using temperature programs were applied to obtain MOF nanoparticles from supersaturated crystallization solutions. The temperature program usually has three steps including the incubation of mother solution, the nucleation from the incubated solution at high temperature and the crystal growth at lower temperature. The nanocrystals of MOF-5, IRMOF-3, and HKUST-1 were synthesized by using temperature programs. The homogeneous MOF-5, IRMOF-3 nanocrystals were generated by the controlled nucleations and crystal growths of these MOFs in the presence of CTAB.[152] In contrast, the HKUST-1 particles up to 200 nm in size accompanying the forming nuclei were observed within a 10 min period of the crystal growth because the nucleation of HKUST-1 overlapped with their crystal growth.[162]

Metal source affects significantly on the formation of MOF nanoparticles. Horcajada *et al.* investigated three iron salts including iron(III) nitrate, iron(III) chloride and iron(III) acetate for the synthesis of iron-based MIL-89 nanoparticle in ethanol solution.[163] While the precipitate of iron muconate MIL-89 appeared immediately in case of the nitrate and chloride salts, the use of iron acetate led to the formation of MIL-89 nanoparticles. It was assumed that iron acetate clusters contained metal-coordinated acetate moieties that acted as modulators suppress the extended crystallization for the formation of MIL-89 nanocrystals.

The concentration of reactants has significant effect on the size of MOF crystals. Khan *et al.* showed that the size of MIL-101 crystals decreased from submicro- to nano-scale with a dilution of the aqueous reaction mixture by water.[164] The decrease in MIL-101 crystal size in the diluted reaction mixtures was explained by a great reduction of the crystal growth rate compared with small reduction of the nucleation rate. Similarly, the addition of water in the reaction mixture of Zr-based MOFs led to a decrease in the nanocrystal size.[165] The dilution of the stable mother liquor of HKUST-1 with a counter solvent induced the formation of the nanocrystals.[166] The stable mother liquor of HKUST-1 was first obtained by mixing copper acetate, BTC and a large amount of dodecanoic acid as modulator in butanol. The cubic HKUST-1 submicro-crystals with a size of 614 ± 11 nm were obtained from the concentrated mother liquor (concentration of BTC, c = 31.2 mM, and dilution

factor, ethanol/mother liquor, d = 1). In contrast, the highly diluted solution (c = 7.9 mM, and d = 8) produced the smaller nanocrystals of 138 ± 1 nm in size. The formation of the smaller HKUST-1 nanocrystals in the diluted solution was attributed to the fast nucleation that contrasted the slow nucleation in the concentrated solution.

The investigation of Khan *et al.* illustrated that high pH values were helpful to decrease the size of MIL-101 nanocrystals.[164] It was assumed that the high pH accelerated the deprotonation of BDC acid into benzenedicarboxylate, resulting in high nuclei concentration that led to small MIL-101 nanocrystals. Similarly, the addition of ammonium hydroxide to vary pH value was used for the control of the crystal size of zirconium-based UiO-66 nanoparticles (UiO standing for University of Oslo).[167] The increase in amount of NH_4OH reduced the crystal size of the Zr-MOFs. The formation of zirconium hydroxide or oxide because of the addition of NH_4OH was also attributed to the formation of the small UiO-66 nanocrystals. However, the change of the pH value of reaction medium can lead to the formation of different MOF structures from identical precursors.[156]

Bataille *et al.* recently demonstrated the effect of solvents on the size of crystalline 1D tubular MOF built from Cu^{2+} ions, 1,2-bis(4-pyridyl)ethane and p,p′-diphenyl-diphosphinate.[168] Under mild conditions, the elongated nanorods with a well-defined range of lengths and cross sections were formed in ethanol, whereas the needle microcrystals were crystallized in water. In another research, the use of water or methanol for the synthesis of MIL-88A nanocrystals led to the larger nanoparticles when compared to the use of DMF.[159] This was related to the higher solubility of fumaric acid (the organic linker of MIL-88A) in DMF rather than in methanol and water as well as the higher dipolar moment of DMF.

2.3.5 Top-down approach

Li *et al.* used a top-down delamination for fabricating crystalline MOF nanosheets from the bulk crystals of layered MOF-2 $[Zn_2(BDC)_4(H_2O)_2{\cdot}2DMF]_n$.[169] The structure of MOF-2 is constructed from zinc square paddle-wheel SBUs and BDC acids. The connection between

the zinc square paddle-wheel SBUs and BDC acids creates 2D layers that are held together by hydrogen-bonding interactions to form MOF-2 framework. The breakage of these hydrogen bonds via an exfoliation resulted in the crystalline MOF nanosheets with thickness ranging from a single layer to multi-layers. Under ultrasonic treatment in acetone at room temperature, the resulted nanosheets had a thickness of 1.5 – 6.0 nm, corresponding to the thickness of two layer to several layers of MOF-2.

2.3.6 Potential application of MOFs involving nanosize

2.3.6.1 Adsorption and heterogeneous catalysis

The reduction of MOF crystal size to the nanometer scale results in a dramatic decrease in diffusion length and increase in accessible active sites as compared to the bulk counterparts. These lead to improving adsorption as well as more efficient catalytic performance of MOF nanoparticles.

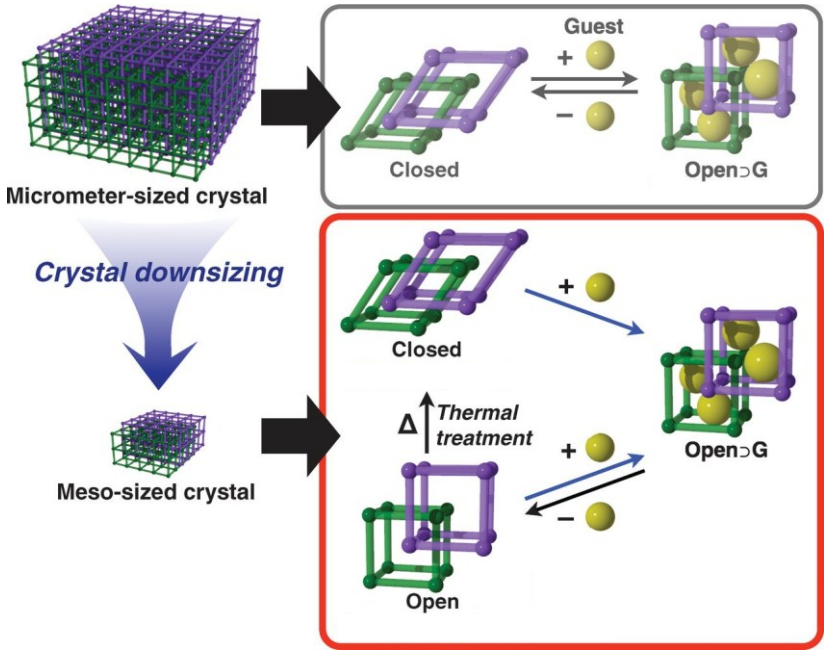

Figure 2.23 Schematic illustration of the structural transformation of flexible $[Cu_2(bdc)_2(bpy)]_n$ PCP. Top: Nonporous closed and guest-included open phases. Bottom: Novel open empty phase was observed with the crystal downsizing. Reproduced with the permission of Science.[150]

Groll *et al.* demonstrated that the methanol adsorption kinetics of flexible $[Zn(ip)(bpy)]_n$ MOF accelerated dramatically with the crystal downsizing.[158] The shape of the sorption isotherm of $[Zn(ip)(bpy)]_n$ MOF varied considerably from the bulk to the nanocrystal though the overall adsorption capacities were almost identical. It is known that flexible PCPs change their structures in response to molecular incorporations but recover their original configurations after the incorporated guests are removed.[150] Therefore, the crystal downsizing can suppress the structural mobility of the flexible PCPs. Kitagawa *et al.* illustrated that the crystal downsizing of twofold interpenetrated structure of $[Cu_2(bdc)_2(bpy)]_n$ MOF induced a novel structural flexibility (Figure 2.23).[150] In addition to two intrinsic phases that were generated by sorption process (i.e., a nonporous closed phase and a guest-included open phase), a new open empty phase that was not observed in case of the bulk counterpart was isolated when downsizing the crystals to the nanoscale. The induction of such molecular-scale shape-memory effect could be exploited as intelligent functional materials that respond to the microscopic environmental changes.

Table 2.2 Catalytic activity of the bulk microcrystals and the nanocrystals of HKUST-1 in the oxidative dehydrogenation of dibenzylamine to dibenzylimine.[170]

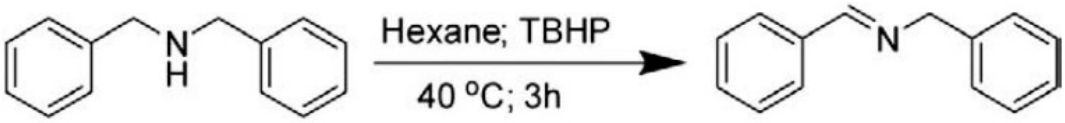

Catalyst	Conversion (%)	Yield (%) [(c)]	TOF (h^{-1}) [(d)]
bulk	17	15	0.8
nanocrystal-A [(a)]	27	24	1.3
nanocrystal-B [(b)]	53	41	2.5

[a] Prepared in the presence of polymer poly(acrylic acid sodium salt).

[b] Prepared in the presence of both polymer poly(acrylic acid sodium salt) and CTAB.

[c] The other product is benzaldehyde.

[d] TOF was calculated by dividing the molar amounts of dibenzylamine converted in 3 h by the molar amounts of Cu used.

The catalytic activity of porous MOFs depends on the particle size that determines the concentration of accessible catalytic sites and the diffusion distance in the pore system. Jiang *et al.* demonstrated that the downsizing of HKUST-1 crystals from the micrometer to nanometer scale enhanced greatly the catalytic performance in the oxidation of dibenzylamine to dibenzylimine.[170] HKUST-1 catalysts with a crystal size less than 200 nm had higher oxidation activity up to three times rather than the bulk of 10 – 20 μm in the crystal size (Table 2.2).

2.3.6.2 Hierarchical structure assembly

The fabrications of MOF films by assembly of preformed MOF nanocrystals have been reported. The resulted films have a hierarchically porous structure consisting of micropores of MOF nanocrystals and mesopores formed by inter-nanoparticles voids. Such hierarchically porous structure facilitates the diffusion and permeation of guest molecules through MOF films. Therefore, the MOF films can be employed as smart separation membranes, chemical sensors or nanodevices.

Ferey *et al.* prepared MOF thin films from preformed MIL-101 nanoparticles by using a dip-coating method.[171] The homogenous colloidal MIL-101 nanocrystals with an average diameter of 22 nm were first produced by using a microwave-assisted synthesis. The nanoparticles in a colloidal solution were then deposited on bare silicon wafer. The thickness of the film depended on the concentration of the suspension and was controlled by the number of dip-coating cycles. The thin films could be used as sensors for vapors due to the selective adsorption property of MIL-101.

The flexible MIL-89 nanoparticles were also used for the assembly of MOF thin film by using the similar dip-coating method.[163] The homogeneous colloidal MIL-89 nanoparticles with a size varied from 20 to 40 nm were synthesized in ethanol media with the presence of acetate moieties as modulator. The thin films were then prepared via the deposition of the nanoparticles on silicon wafers. Each dip-coating process deposited a single layer of the

colloid on the substrate. Therefore, the film thickness could be increased and controlled through repetition of the dip-coating process.

Recently, the crack-free films of amine-functionalized MIL-101 have been fabricated by dip-coating of the nanoparticles in the presence of polyethylenimine (PEI).[172] The suspensions of MIL-101–NH_2 nanoparticles were first fabricated in ethanol containing PEI. The films were then prepared by dip-coating Anodiscs (anopore alumina) in the suspension a number of times. The presence of PEI in the suspension enhanced the interaction of MIL-101–NH_2 nanoparticles with the surface of Anodisc through hydrogen bonding, which helped the nanoparticles to be homogeneously adsorbed on the surface during the dip-coating. In addition, the PEI molecules on the MIL-101–NH_2 nanoparticles reduced and homogenized the stress forces between the nanoparticles, which contributed to the formation of the crack-free films. The films exhibited high selectivity for CO_2 over N_2 and high CO_2 capacity, which offered an efficient separation of CO_2 from N_2.

Glass-supported $Eu_{1-x}Tb_x$–MOF films were fabricated from the suspension of the pre-synthesized MOF nanocrystals by using a spin-coating method.[151] $Eu_{1-x}Tb_x$–MOF nanocrystals were synthesized by coordination modulation approach using monocarboxylate salts as modulators. The film thickness was controlled by the nanocrystal concentration in the suspension and the spin-coating rate. The films had strong luminescence property and efficient Tb^{3+}–to–Eu^{3+} energy transferability. Therefore, they were potential candidates for applications in the field of color displays, luminescence sensors and structural probes.

The preparation of porous MOF thin films on the inner walls of capillary columns for GC separations has been reported. Gu and Yan fabricated MIL-101 coated capillary silica column for the high-resolution GC separation of xylene isomers and ethylbenzene by using a dynamic coating method (Figure 2.24).[173] The suspension of MIL-101 nanocrystals was first filled into the capillary column under gas pressure, and then pushed through the column to leave a wet coating layer on the inner wall. The capillary column was further treated using a temperature program before the GC separation experiment. By using the

same dynamic coating process, Yan *et al.* have recently fabricated IRMOF coated-capillary columns from IRMOF-1, IRMOF-3 nanocrystals for the high-resolution GC separation of persistent organic pollutants.[174]

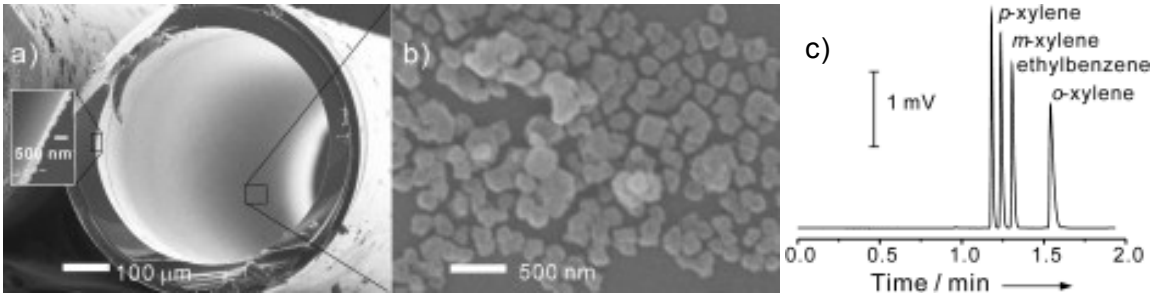

Figure 2.24 The thin film of MIL-101 on the inner wall of capillary silica column and the GC separation of xylene isomers and ethylbenzene of the coated capillary column. Reproduced with the permission of Wiley InterScience.[173]

2.3.6.3 Biomedical application

MOFs suitable for biomedical applications must have biologically friendly compositions and be stable under biological conditions.[87] The biocompatible metal cations are Ca, Mg, Zn, Fe, Ti, or Zr whose oral lethal doses 50 (LD_{50}) range from a few µg/kg up to more than 1 g/kg (calcium). Meanwhile, the common linkers are exogenous compounds such as polycarboxylates which do not intervene in the body cycles. The incorporation of functional groups on these linkers can modulate the host-guest interactions, allowing a better control of drug release. The other linkers are endogenous compounds such as gallic, fumaric and muconic acids. The endogenous linkers might be used in the body, which would strongly decrease the risk of adverse effects. The imaging property of MOFs as contrast agents in magnetic resonance imaging, optical imaging or X-ray computed tomography allows following both detection of the drug-loaded nanoparticles and efficiency of a given therapy. The prerequisite for medical applications is the preparation of homogeneous and monodispersed MOF nanoparticles because some administration routes such as systemic circulation require precise nanoscale sizes.

Variety of nanoscale MOFs have been tested as drug-delivery nanocarriers and contrast agents.[175] Among them, the non-toxic iron-carboxylate MOFs such as MIL-53, MIL-88A, MIL-88B, MIL-89, MIL-100 and MIL-101–NH_2 are shown as potential candidates for these purposes.[160] In addition to the advantage of high pore volume and large surface area for high drug loading capacity and efficient delivery of drugs in the body, these MOF nanoparticles are synthesized in biologically favourable aqueous or ethanol media with controlled particle sizes. The surface of the nanocrystals can be engineered to achieve suitable stability, bio-distribution and targeting abilities (Figure 2.25). Furthermore, the paramagnetic iron atoms, free and coordinated water molecules in the networks of these MOF nanoparticles allow them be effective contrast agents.

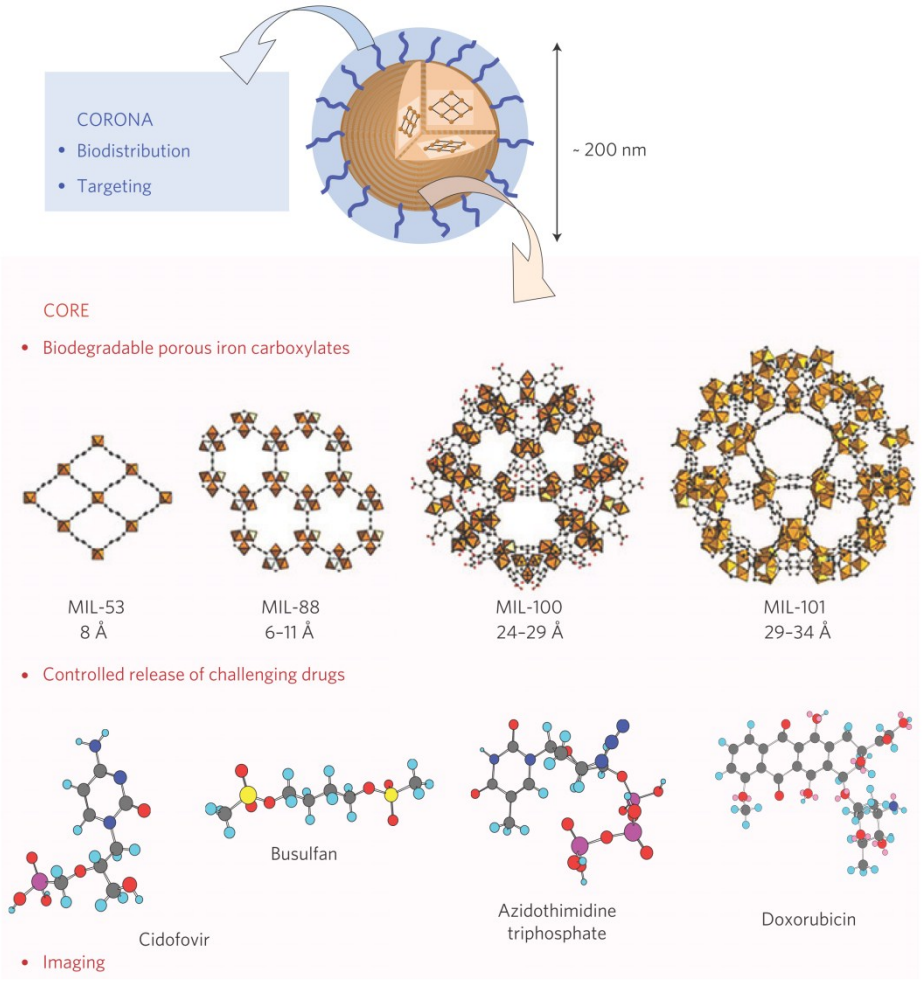

Figure 2.25 Scheme of engineered core–corona iron carboxylate MOFs for drug delivery and imaging. Reproduced with the permission of Nature Publishing Group.[160]

Nanosized Gd- and Mn-based MOFs have also been reported as potential contrast agents in magnetic resonance imaging.[176] The paramagnetic metal ions enhance image contrast by increasing the rate of water proton relaxation when a magnetic field is applied. Moreover, the nanosized MOFs can be doped with emissive lanthanide ions to afford optical property for imaging applications.

2.3.6.4 Templates

The use of nanosized MOFs as templates for the synthesis of core-shell nanostructures was reported. The metal oxide shells such as silica and titania were coated on several nanosized MOFs. Lin *et al.* prepared silica shells with variable thickness on $Ln(BDC)_{1.5}(H_2O)_2$ nanocrystals (Ln = Eu^{3+}, Gd^{3+}, Tb^{3+}) by using sol-gel procedure.[176] The nanocrystals were first functionalized with polyvinylpyrollidone to reduce particle aggregation in solution, followed by a treatment with tetraethylorthosilicate (TEOS) in an ammonia/ethanol mixture. The shell thickness was tuned by varying the reaction time or the amount of TEOS. The MOF core and silica shell nanostructures were functionalized with medical agents for biomedical applications.[177] The MOF core could be removed by dissolving at low pH to fabricate hollow silica nanoparticles. Recently, amorphous titania shell has been deposited on MIL-101 nanocrystals by using acid-catalyzed hydrolysis and condensation of titanium(IV) bis(ammonium lactato)dihydroxide in water at room temperature.[178] The thickness of the titania shell could be varied by variation of the concentration of HCl acid as catalyst for the hydrolysis and condensation or by the reaction time. The subsequent calcination of this structure generated a composite of mixed metal oxides as a catalyst.

2.4 Photocatalytic water splitting

Water splitting to generate H_2 and O_2 using solar energy in the presence of semiconductor photocatalysts has revealed a potential means of clean, renewable fuel production.[179-181] Photocatalytic semiconductor has a band structure in which the conduction band (CB) is separated from the valence band (VB) by a band gap. When a semiconductor photocatalyst is illuminated by light with energy equal to or larger than that of the band gap, the electrons

are excited from the VB into the CB, leaving positive holes in the VB. The photogenerated electrons and holes can participate in redox reactions.

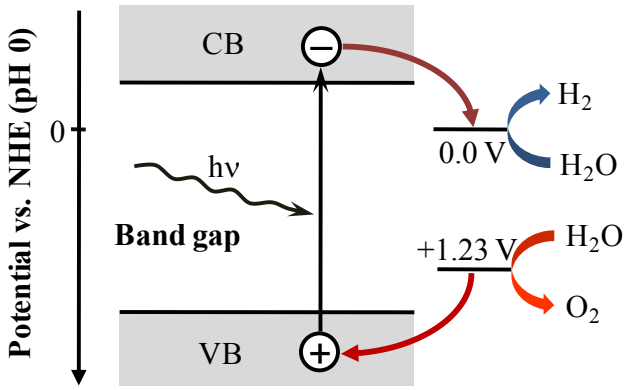

Figure 2.26 Principle of water splitting using semiconductor photocatalysts

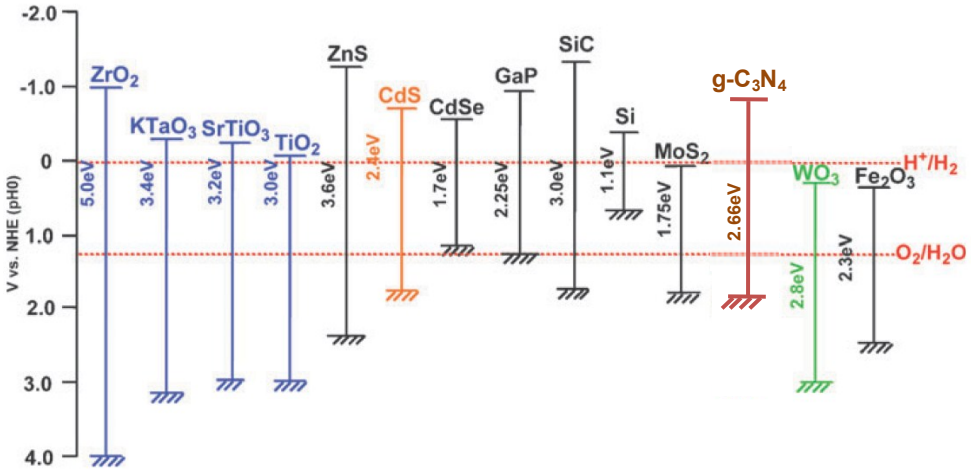

Figure 2.27 Relationship between the band structure of semiconductors and the redox potential of water splitting.[182,183]

In water splitting, water molecules are reduced by photogenerated electrons to generate H_2 and are oxidized by photogenerated holes to produce O_2 (Figure 2.26). To induce water splitting, the bottom level of the CB must be more negative than the redox potential of H^+/H_2 (0.0 V vs. NHE at pH = 0) while the top level of the VB must be more positive than

the redox potential of O_2/H_2O (+1.23 V vs. NHE at pH = 0).[182] In principle, various semiconductor materials have the levels of CB and VB suitable for water splitting (Figure 2.27). However, the band gap should be narrower than 3.0 eV for the visible light-driven photocatalysis ($\lambda > 415$ nm).

The surface separation of the photogenerated electrons and holes is required to achieve efficient water splitting. The downsizing of the particle size of the photocatalysts shortens migration of the electrons and holes toward surface active sites, resulting in a significant decrease in the recombination probability. However, the small nanoparticle size can generate a quantum size effect that widens the band gap.[184] The recombination between photogenerated electrons and holes is dominant if the photocatalytic surface does not have active sites for the redox reactions. Therefore, nanoparticulate cocatalysts such as Pt, Rh, NiO_x and RuO_2 for H_2 evolution and Co_3O_4, Mn_3O_4 for O_2 evolution are loaded to form active sites on the surface of photocatalysts.[179,185] In addition, the physical separation between the distinct active sites for the reduction and oxidation reactions enhances the water splitting activity.[186]

The backward reaction forming water from evolved H_2 and O_2 is one of the reasons leading to inefficient overall water splitting. Therefore, sacrificial reagents (hole or electron scavengers) are usually used for half reactions of water splitting to produce either H_2 or O_2.[187] In the half reaction for H_2 evolution, photogenerated holes in the VB oxidize hole scavenger such as alcohols, S^{2-} and SO_3^{2-} ions instead of water. This enriches photogenerated electrons in the CB, and thus H_2 evolution reaction is enhanced.[182] In contrast, photogenerated electrons in the CB are consumed by electron scavenger such as Ag^+ and Fe^{3+} ions in the half reaction for O_2 evolution, resulting in an enhancement of O_2 evolution reaction.

Metal oxide, sulfide, nitride and graphitic carbon nitride (g-C_3N_4) photocatalysts have been developed for water splitting.[182,183,188,189] For example, CdS with suitable band structure is an excellent photocatalyst for H_2 evolution under visible light in the presence of hole scavengers.[190-192] However, the photocorrosion in which S^{2-} in CdS rather than H_2O is

oxidized by photogenerated holes makes CdS inactive for overall water splitting and decreases the stability of the photocatalyst.[193] On the other hand, WO_3 catalyzes efficiently the half reaction for O_2 evolution under visible light in the presence of electron scavengers, but is inactive for H_2 evolution due to the CB level more positive rather than the redox potential of H^+/H_2.[194,195] g-C_3N_4 and its modified derivatives also exhibit photocatalytic activity for water reduction into H_2 or water oxidation into O_2 in the presence of a proper hole or electron scavenger under visible light irradiation.[183,196,197]

Among the semiconductor photocatalysts, titania material has revealed as the most promising candidate because of inexpensive, non-toxic and robust photocatalyst under photochemical conditions. However, the wide band gap (3.0 eV for the rutile phase and 3.2 eV for the anatase phase) makes pristine TiO_2 only active under UV light that is only a small fraction of the solar light spectrum. Therefore, the modifications are required to induce the photon absorbance within the visible light region.[184,198,199] These processes include modifications of chemical composition such as doping with transition metal ions (e.g., V, Cr, Mn, Fe, Ni) or with nonmetallic elements (e.g., N, S, C, B, F, Cl, Br); and surface chemical modifications such as sensitizing with organic dyes,[200] metal nanoparticles,[201,202] or narrow band gap semiconductors.[203,204] In general, the substitution of transition metals for the Ti sites (metal-doping) seems to be easy while the replacement of nonmetallic elements for the O sites (nonmetal-doping) is more difficult due to differences in charge states and ionic radii. The small size of the nanoparticle is beneficial for the doping. Moreover, the activity of TiO_2 materials depends on their primary particle size and shape.[205] Therefore, the progress of TiO_2-based photocatalysts still attracts enormous researches.